Article

Cell Reports

Axonal Odorant Receptors Mediate Axon Targeting

Graphical Abstract

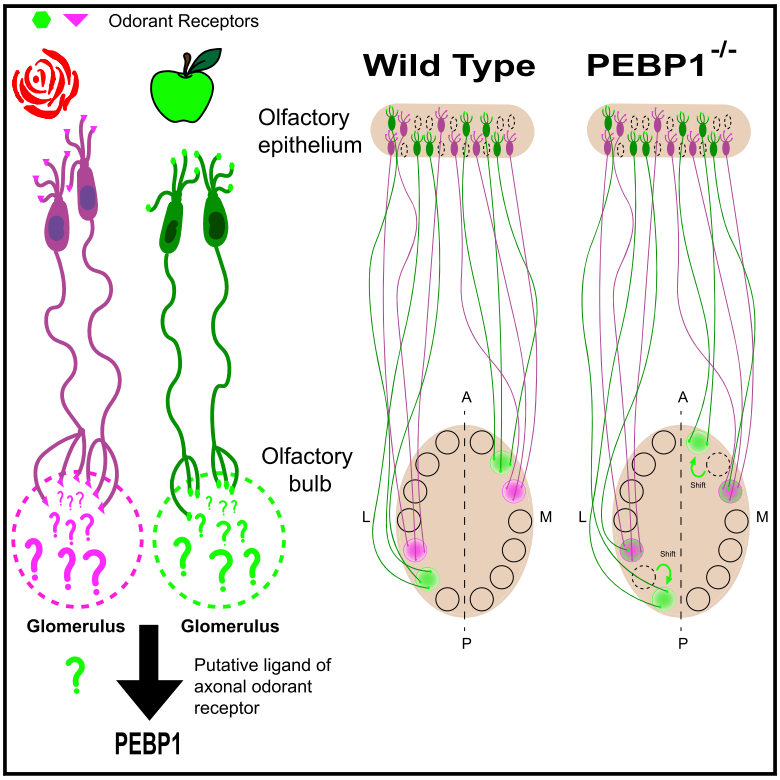

Authors

Ilaria Zamparo, Simona Francia, Sira Angela Franchi, ..., Bart De Strooper, Hiroaki Matsunami, Claudia Lodovichi

Correspondence

claudia.lodovichi@unipd.it

In Brief

Odorant receptors play a critical role in the sensory map formation. Zamparo et al. find that axonal odorant receptors respond to cues expressed in the olfactory bulb. Among these, PEBP1 acts as a putative ligand of axonal receptors, and its genetic ablation results in a disrupted sensory map *in vivo*.

Highlights

- Axonal odorant receptors respond to cues elaborated in the olfactory bulb
- PEBP1, expressed in the olfactory bulb, is a putative ligand of axonal receptors
- Genetic ablation of PEBP1 results in disrupted olfactory map *in vivo*
- Axonal odorant receptors modulate axon targeting in the sensory map formation

Zamparo et al., 2019, Cell Reports *29*, 4334–4348
December 24, 2019
https://doi.org/10.1016/j.celrep.2019.11.099

CellPress

OPEN ACCESS
CellPress

Cell Reports
Article

Axonal Odorant Receptors Mediate Axon Targeting

Ilaria Zamparo,[1,14] Simona Francia,[2,14] Sira Angela Franchi,[2] Nelly Redolfi,[1] Elisa Costanzi,[3] Axelle Kerstens,[4,5,9] Yosuke Fukutani,[6,7] Roberto Battistutta,[3] Patrizia Polverino de Laureto,[8] Sebastian Munck,[4,5,9] Bart De Strooper,[5,9,10] Hiroaki Matsunami,[7,11] and Claudia Lodovichi[2,12,13,15,*]

[1]Department of Biomedical Sciences, University of Padua, Padua, Italy
[2]VIMM, Padua, Italy
[3]Department of Chemical Sciences, University of Padua, Padua, Italy
[4]VIB Bio Imaging Core, Leuven, Belgium
[5]Department of Neurosciences, KU Leuven, Leuven, Belgium
[6]Department of Biotechnology and Life Science, Tokyo University of Agriculture and Technology, Koganei, Tokyo, Japan
[7]Department of Molecular Genetics and Microbiology, Duke University Medical Center, Durham, NC, USA
[8]Department of Pharmaceutical Sciences, University of Padua, Padua, Italy
[9]VIB-KU Leuven Center for Brain & Disease Research, Leuven, Belgium
[10]Dementia Research Institute, UCL, London, UK
[11]Department of Neurobiology, Duke Institute for Brain Sciences, Duke University, Durham, NC, USA
[12]Neuroscience Institute, CNR, Padua, Italy
[13]Armenise-Harvard Foundation CDA, Boston, MA, USA
[14]These authors contributed equally
[15]Lead Contact
*Correspondence: claudia.lodovichi@unipd.it
https://doi.org/10.1016/j.celrep.2019.11.099

SUMMARY

In mammals, odorant receptors not only detect odors but also define the target in the olfactory bulb, where sensory neurons project to give rise to the sensory map. The odorant receptor is expressed at the cilia, where it binds odorants, and at the axon terminal. The mechanism of activation and function of the odorant receptor at the axon terminal is, however, still unknown. Here, we identify phosphatidylethanolamine-binding protein 1 as a putative ligand that activates the odorant receptor at the axon terminal and affects the turning behavior of sensory axons. Genetic ablation of phosphatidylethanolamine-binding protein 1 in mice results in a strongly disturbed olfactory sensory map. Our data suggest that the odorant receptor at the axon terminal of olfactory neurons acts as an axon guidance cue that responds to molecules originating in the olfactory bulb. The dual function of the odorant receptor links specificity of odor perception and axon targeting.

INTRODUCTION

Specificity of connections among neurons is essential to translate sensory information in meaningful neuronal codes. In mammals, sensory neurons in the peripheral sheets typically project their axon to specific loci in the brain in a continuous pattern, such that neighboring peripheral inputs are maintained in the brain. The spatial segregation of sensory afferents provides topographic maps that define the quality and location of sensory stimuli.

The topographic organization of the olfactory system differs in several ways from this paradigm. Each olfactory sensory neuron (OSN) expresses only one type of odorant receptor (OR) from a repertoire of more than one thousand OR genes (Buck and Axel, 1991). In the olfactory epithelium, OSNs expressing a given OR are randomly distributed within overlapping zones along the dorso-ventral axis. Spatial order is achieved in the olfactory bulb (OB), the first retransmission center of the olfactory system, where OSNs expressing the same OR converge to form synapses with postsynaptic neurons at specific loci (e.g., glomeruli) with one glomerulus on the medial and one on the lateral side of each OB (Mombaerts et al., 1996; Ressler et al., 1994; Vassar et al., 1994). This spatial segregation of OSN axons creates a topographic map on the OB, with each glomerulus representing a specific OR. The instructive role of the OR in the convergence of sensory neurons has been demonstrated by genetic experiments in which alteration of the OR coding sequence resulted in an altered sensory map (Feinstein et al., 2004; Wang et al., 1998). The expression (Barnea et al., 2004; Strotmann et al., 2004) and the local translation (Dubacq et al., 2009) of the OR at the axon terminal of OSN suggested that the axonal receptor itself may act as an axon guidance molecule. However, the mechanism of activation and the function of the OR expressed at the axon terminal remain unknown.

At the cilia, the OR binds odorants, resulting in the activation of a specific G protein, G_{olf}, which stimulates adenylyl cyclase III to synthesize cyclic adenosine monophosphate (cAMP). This cAMP binds cyclic nucleotide-gated (CNG) channels, allowing Ca^{2+} and Na^{+} influx (Bradley et al., 2005; Menini, 1999). The OR expressed at the axon terminal is also coupled to cAMP and Ca^{2+} signaling (Lodovichi and Belluscio, 2012; Maritan et al., 2009; Pietrobon et al., 2011). These second messengers play a critical role in axon elongation and turning (Song et al., 1997; Zheng and Poo, 2007), and cAMP was shown to contribute to the coalescence of sensory axons into glomeruli in the OB (Chesler et al., 2007; Imai et al., 2006).

Here, by studying Ca^{2+} dynamics at the axon terminal of OSNs and in HEK cells expressing a specific OR, we found evidence that molecules expressed in the OB activate the ORs at the axon terminal and modulate OSN axon turning. Among this pool of molecules, we identified phosphatidylethanolamine-binding protein 1 (PEBP1) (NP_058932.1) as a putative ligand that activates ORs at the axon terminal and affects the turning behavior of sensory axons. In mice carrying a null mutation of PEBP1, the topographic organization of the OB is deeply perturbed. We suggest that the axonal ORs may act as axon guidance molecules activated by cues expressed in the OB to direct the formation of the sensory map.

RESULTS

Molecules Expressed in the Olfactory Bulb Activate the Odorant Receptors Expressed at the Axon Terminal of Olfactory Sensory Neurons

To identify molecules in the OB that could activate the axonal OR, we generated an OB dialysate (from embryonic rat OBs; see STAR Methods) and tested its effect on different ORs by studying the dynamics of Ca^{2+} at the axon terminal of embryonic rat OSNs. We obtained several fractions of OB dialysate by size-exclusion chromatography (SEC). The third peak of SEC (SEC-3) was the only one that elicited Ca^{2+} rises at the axon terminal in OSNs (Figures 1A and 1C). We further fractionated SEC-3 by ionic exchange chromatography (IEC) and found 2 peaks (IEC-1 and IEC-2) that elicited Ca^{2+} rise as shown (Figures 1B, 1C, and S1A).

To ascertain that this Ca^{2+} rise was caused by OR activation, HEK293T cells were transfected with different ORs (OREG, S6, and Olfr62) and loaded with the fura-2 Ca^{2+} indicator (see STAR Methods). HEK293T cells not expressing ORs did not exhibit a rise in Ca^{2+} upon stimulation with IEC-2 or with odor (Figure 1D). However, when expressing distinct ORs, they respond promptly with a Ca^{2+} rise upon challenge with IEC-2 or with their corresponding odor ligands (Figures 1E–1I). In contrast, IEC-1 exhibited a Ca^{2+} rise, even in the absence of OR expression (Figures S1B and S1C), and was not further investigated.

IEC-2 also elicited Ca^{2+} response when applied to mouse OSN axon terminals (Figures 1J–1L), although buffer solution alone did not elicit Ca^{2+} responses neither in sensory neurons nor in HEK293T cells expressing OR (Figures S1D–S1G).

Ligand-dependent OR activation is coupled to Ca^{2+} influx via cyclic nucleotide-gated channel opening activated by cAMP (Figure S1H). Upon IEC-2 application at the axon terminal, a prompt cAMP rise was observed locally (Figures S1I and S1J). To ascertain the origin of Ca^{2+} influx upon stimulation with molecules from the OB, OSNs were stimulated with IEC-2 in presence of SQ22536, an inhibitor of adenylyl cyclase. Ca^{2+} rise was practically abolished, indicating that Ca^{2+} influx at the axon terminal depends on cyclic nucleotide-gated channel activation (Figures S1K–S1M). When denatured with heat, IEC-2 was no longer capable of inducing a Ca^{2+} rise (Figures S1N and S1O), suggesting that the active pool of molecules from the OB is proteinaceous in nature.

PEBP1, a Putative Ligand for the Odorant Receptor Expressed at the Axon Terminal of Olfactory Sensory Neurons

We further fractionated IEC-2 by reverse-phase chromatography (RPC). All peaks were tested on OSNs. Peaks 23 and 35 of RPC elicited a prompt Ca^{2+} rise in OSNs (Figures S2A–S2C) and were used to stimulate HEK293T cells (Figures S2D–S2F) expressing OREG, the most responsive OR to unfractionated IEC-2 (Figures 1E and 1I). The two peaks were analyzed by mass spectrometry. Among the identified proteins, PEBP1, also known as Raf kinase inhibitory protein 1 (RKIP-1), was present in both peaks (Tables S1 and S2). PEBP1 is an ~21-kDa protein that belongs to a highly conserved family of proteins that are expressed in numerous tissues and cell types in a variety of species (Al-Mulla et al., 2013; Granovsky and Rosner, 2008). In rodents, PEBP1 is expressed in several brain areas, both in neurons and in non-neuronal cells (Frayne et al., 1999; Theroux et al., 2007). The physiological function of PEBP1 in the brain has remained elusive. Given its low molecular weight, ability to be secreted, G-protein coupled receptor modulating activity (Goumon et al., 2004; Granovsky and Rosner, 2008), and the presence of olfactory deficits in mice carrying a null mutation for PEBP1 (Theroux et al., 2007), we hypothesized PEBP1 to be an OR ligand.

To assess the ability of PEBP1 to modulate Ca^{2+} levels at the OSN axon terminal, we applied PEBP1 locally to the axons of OSNs loaded with the Ca^{2+} indicator fura-2. Rat and mouse OSNs exhibited a prompt Ca^{2+} rise at the axon terminal (Figures 2A–2D). To ascertain that the Ca^{2+} rise observed in OSNs in response to PEBP1 was due to OR activation, HEK293T cells transfected with specific ORs (OREG, P2, S6, Olfr62, and M72) and loaded with fura-2 were challenged with PEBP1 and the corresponding odor ligands or carbachol in the case of P2 OR, whose corresponding odor is still unknown. A prompt Ca^{2+} rise was observed in response to PEBP1 only in HEK293T cells expressing OR and not in HEK293T cells expressing the empty vector, chaperone proteins (Receptor transporting protein family members, RTPs), and $G_{\alpha 15}$ (Figures 2E–2G and 2I). HEK293T cells expressing the OR M72 did not exhibit Ca^{2+} rise in response to PEBP1, although they did respond to the corresponding odor (Figures 2H and 2I). This indicates that there are likely other ligands regulating sensory afferent segregation in the OB of, e.g., M72-expressing neurons, in line with previous speculations that a limited number of different ligands could be involved in this guidance process (Barnea et al., 2004; Wang et al., 1998). To ascertain the specificity of the response to PEBP1, HEK cells expressing specific ORs were treated with PEBP1 in presence of Proteinase K in order to inactivate proteins. In this condition, no Ca^{2+} rise was observed. When the same HEK cells were stimulated (after washing away PEBP1+ ProtK) with PEBP1 followed by cognate odor ligands, prompt Ca^{2+} responses were observed in response to all these stimuli (Figures S2G, S2H, and S2K). To eliminate the possibility that substances introduced in the purification steps are activating the OR, we purified cyclin-dependent kinase 2 (CDK2) using the same procedure used to purify PEBP1. HEK cells expressing specific ORs and loaded with fura-2 exhibited no Ca^{2+} rise in response to CDK2. The same

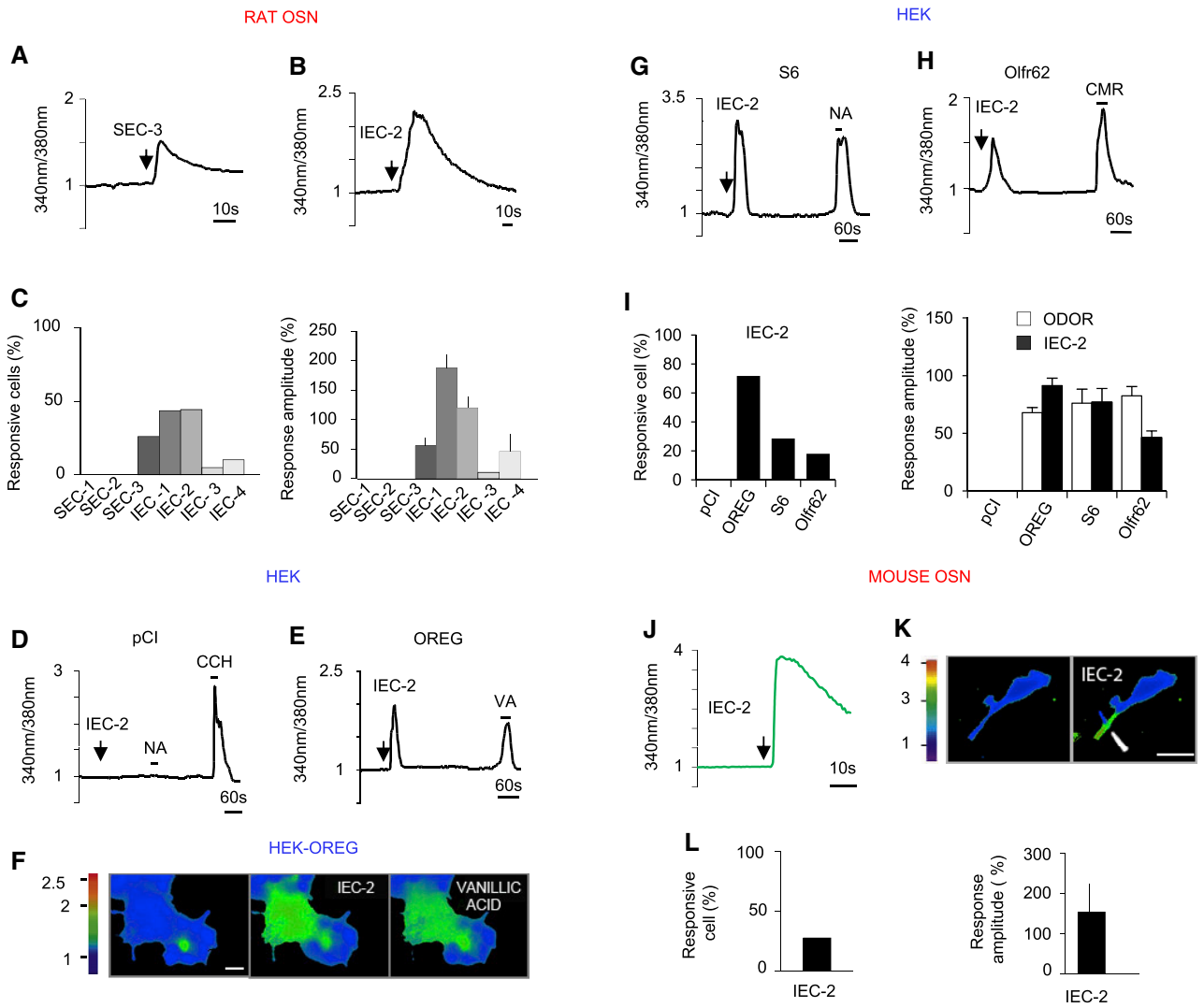

Figure 1. Ca^{2+} Dynamics in Olfactory Sensory Neuron (OSN) Axon Terminals and HEK293T Cells in Response to Molecules from the Olfactory Bulb (OB)

Fura-2 Ca^{2+} imaging.

(A and B) Embryonic rat OSN axon terminals exhibit a prompt Ca^{2+} rise upon stimulation with the third peak of size-exclusion chromatography (SEC-3) (A) and with the second peak of ionic-exchange chromatography (IEC-2) (B).

(C) Summary of results (SEC-1, n = 21; SEC-2, n = 20; SEC-3, n = 31; IEC-1, n = 92; IEC-2, n = 97; IEC-3, n = 20; IEC-4, n = 20). Bars represent SEM.

(D) HEK293T cells not expressing odorant receptor (OR) (pCI = empty vector; n = 76) do not exhibit Ca^{2+} response to IEC-2 or to odors (nonanedioic acid [NA]). A prompt Ca^{2+} rise is present in response to carbachol (CCH) (used as control).

(E, G, and H) HEK293T cells expressing ORs exhibit Ca^{2+} rise in response to IEC-2 and the corresponding odor. OREG-vanillic acid (VA) (E; n = 72), S6-nonanedioic acid (NA) (G; n = 63), and Olfr62-2-coumaranone (CMR) (H; n = 122) are shown.

(F) Sequence of pseudocolor images of HEK293T cells expressing OREG, showing the changes in [Ca^{2+}] before and upon stimulation with IEC-2 and with VA. Scale bar, 20 μm.

(I) Summary of results of Ca^{2+} dynamics in HEK cells. Bars represent SEM.

(J) Ca^{2+} response to IEC-2 in a mouse OSN axon terminal.

(K) Pseudocolor images of the mouse OSN, showing changes in [Ca^{2+}] before and after IEC-2 stimulation, locally at the axon terminal (arrowhead). Scale bar, 20 μm.

(L) Summary of results (n = 18). Bar represents SEM.

HEK cells exhibited, after washing away CDK2, a prompt Ca^{2+} transient when stimulated only with PEBP1. A Ca^{2+} increase was observed in response to the subsequent stimulation with the cognate odor ligand, vanillic acid, or with carbachol in cases with HEK cells expressing the P2 OR, due to the absence of a known ligand for this OR (Figures S2I–S2K). Ringer's solution did not elicit any Ca^{2+} response in HEK cell transfected with specific ORs. The same HEK cells exhibited a prompt Ca^{2+} rise in response to the cognate odor ligand vanillic acid (VA) and to PEBP1 (Figure S2L).

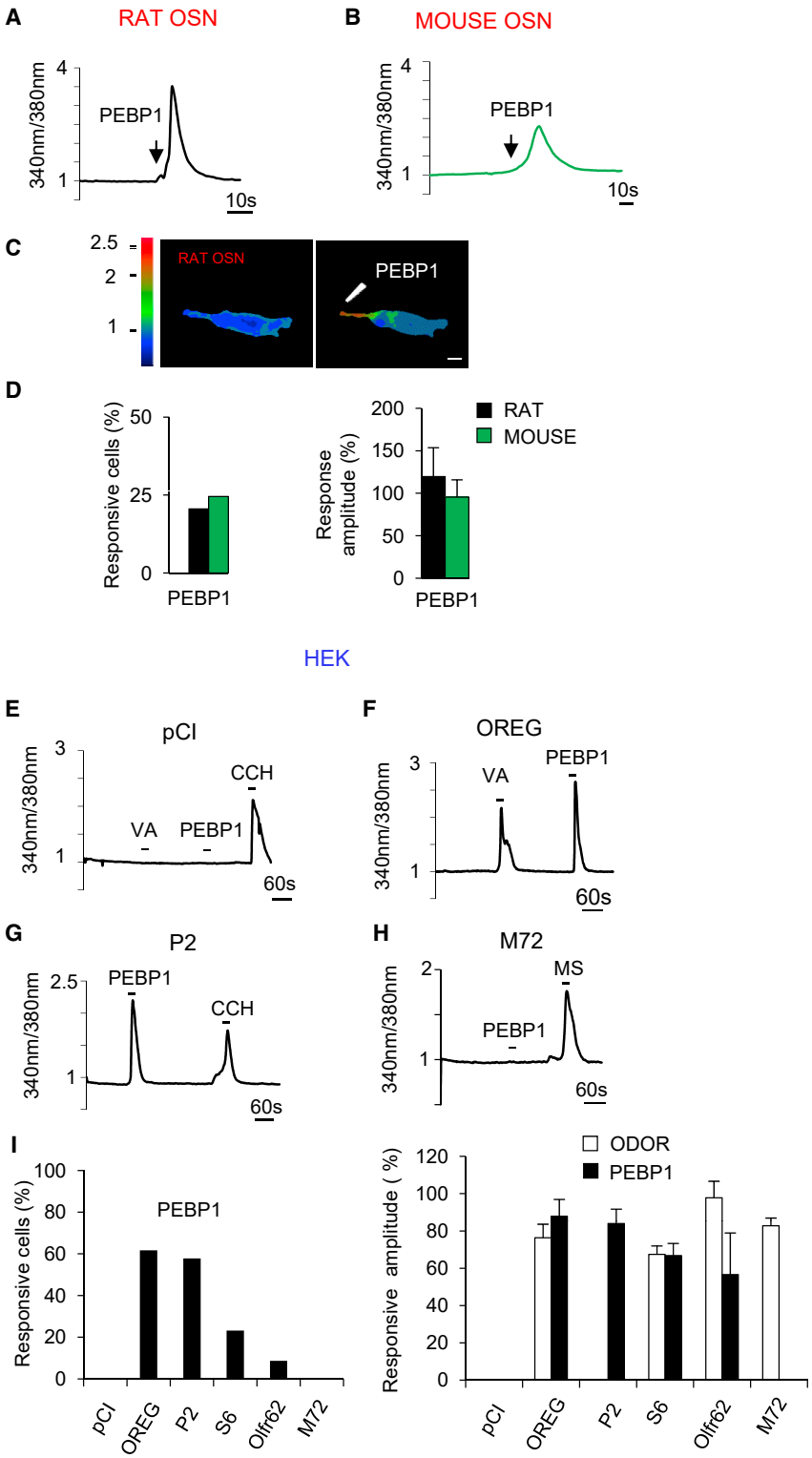

Figure 2. Ca^{2+} Dynamics in Rat and Mouse OSN Axon Terminals and HEK293T Cells in Response to Phosphatidylethanolamine-Binding Protein 1 (PEBP1)

Fura-2 Ca^{2+} imaging.

(A and B) Normalized fluorescence ratio changes (340 nm/380 nm) at the OSN axon terminals of rat in (A) and mouse in (B), upon stimulation with PEBP1.

(C) Pseudocolor images of the rat OSN, showing changes in [Ca^{2+}] at the axon terminal (arrowhead) before and upon application of PEBP1. Scale bar, 10 μm.

(D) Summary of results. Embryonic rat OSN, n = 72; mouse OSN, n = 57. Bars represent SEM.

(E) HEK293T cells not expressing odorant receptors (ORs) (pCI = empty vector) do not exhibit Ca^{2+} response to odor, e.g., Vanillic acid (VA), or to PEBP1. A prompt Ca^{2+} rise is observed in response to CCH, used as control.

(F–H) Examples of Ca^{2+} dynamics in HEK293Tcells transfected with distinct ORs (F: OREG; G:P2; H:M72) and stimulated with the corresponding odor (VA; methyl salicylate [MS]) or carbachol (CCH) and with PEBP1.

(I) Summary of results (pCI, n = 112; OREG, n = 47; P2, n = 70; S6, n = 112; Olfr62, n = 45; M72, n = 110). Bars represent SEM.

See also Figures S2 and S6 and Tables S1 and S2.

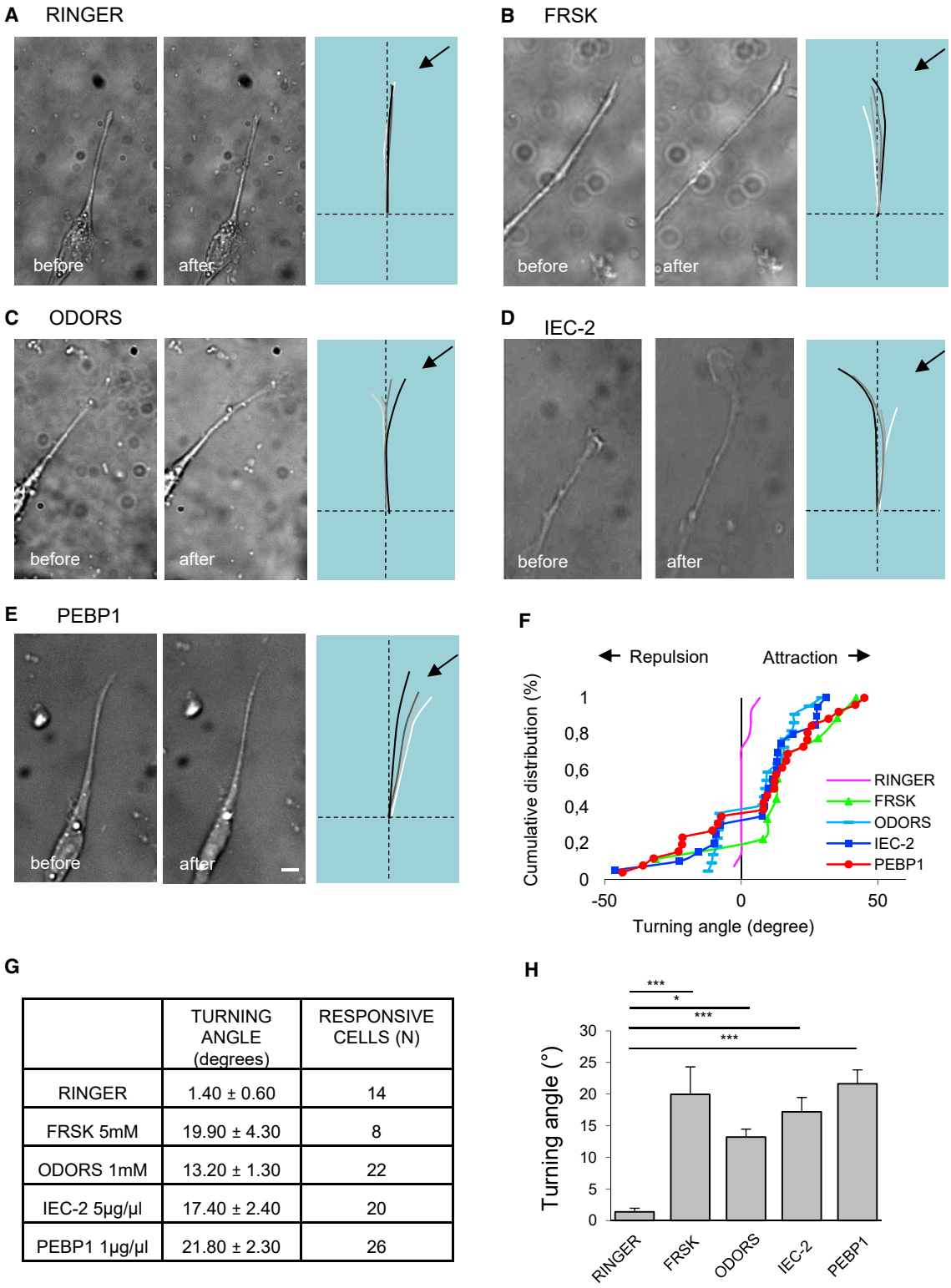

G

	TURNING ANGLE (degrees)	RESPONSIVE CELLS (N)
RINGER	1.40 ± 0.60	14
FRSK 5mM	19.90 ± 4.30	8
ODORS 1mM	13.20 ± 1.30	22
IEC-2 5µg/µl	17.40 ± 2.40	20
PEBP1 1µg/µl	21.80 ± 2.30	26

Figure 3. Turning Response of Rat OSN Axon Terminal in Presence of Chemical Gradients

(A–E) Examples of stop frames of time-lapse imaging of isolated embryonic rat OSN axon terminals at the beginning (left panel) and at the end (central panel) of pulsatile application of chemicals from a glass pipette. Composite drawings (right panel) of the turning responses of neurites during the stimulation period were made by superimposing traces to the video records of the microscopic images. White traces depict the position of the axon terminal at the beginning, although black traces indicate the trajectory of the neurites at the end of the stimulation period (~1 h). Trajectories of the axon terminal at intermediate time points during the

(legend continued on next page)

PEBP1 Modulates Axon Turning Behavior of Rat Olfactory Sensory Neurons

Axon guidance signals steer the direction of growth cones. To ascertain whether PEBP1 could regulate axon turning, we performed time-lapse imaging of rat OSN axon terminals (Lohof et al., 1992). Microscopic gradients are generated by pulsatile ejections of molecules able to modulate cAMP and/or Ca^{2+} levels at the axon terminal. We found that neurite direction (see STAR Methods for details) was affected by IEC-2 and PEBP1 (Figures 3 and S3), similar to the effects of pharmacological agents, such as forskolin, a generic activator of adenylyl cyclase III, and odors known to modulate cAMP and Ca^{2+} at the olfactory sensory neuron axon terminal (Maritan et al., 2009). All together, our data suggest that PEBP1 can induce Ca^{2+} rise at the OSN axon terminal via OR activation and modulate neurite direction.

To investigate whether PEBP1 is expressed in locations suitable to modulate the targeting of incoming axons, *in vivo*, we performed immunostaining using a PEBP1 antibody in coronal sections of rat and mouse OBs (Figures 4 and 5).

PEBP1 is highly expressed in periglomerular cells that enwrap each glomerulus and establish contacts with the incoming axons. PEBP1-positive cells were detected mostly in the anterior, medial, and lateral side of each OB, although in the posterior side, PEBP1 expression is very low. This pattern of PEBP1 expression resulted in a global gradient of PEBP1 along the antero-posterior axis (Figures 4B, 4H, 4K, 4N, 5A–5D, and 5K). At the local level, however, glomeruli enwrapped by cells expressing high levels of PEBP1 were intermingled with glomeruli around which PEBP1 could hardly be detected, giving rise to a patchy distribution of PEBP1 in circumscribed areas (Figures 4C, 4E, 4F, 4I–4L, and 5E–5G). PEBP1 expression was not found in the OB of PEBP1$^{-/-}$ mice (Figures 5J and 5K). The expression of PEBP1 in the OB was confirmed by RT-PCR and western blot (Figures S4U and S4V). PEBP1 was not expressed in OSNs, as revealed by RT-PCR and immunostaining sections of the epithelium (Figure S4). According to the latter results, PEBP1 expression was not detected in the axon terminals of OSNs that form glomeruli (Figure S5).

The Olfactory Map Is Altered in PEBP1 Mutant Mice

If PEBP1 is involved in OSN axonal convergence to form glomeruli in the OB, giving rise to the sensory map, mice carrying a null mutation for PEBP1 should exhibit altered spatial segregation of sensory afferents. We obtained mice homozygous for a null mutation in PEBP1 (PEBP1$^{-/-}$ mice; Theroux et al., 2007) and crossed them with homozygous lines of mice where OR expression leads to expression of fluorescent proteins, allowing for the visualization of the ORs corresponding glomeruli in the OB. We choose the P2 OR because it exhibited a prompt Ca^{2+} response to PEBP1 in our previous assays. The OR M72, which was not responsive to PEBP1 in our previous experiments, was used as a negative control (Figures 2G–2I). To further corroborate the activation of P2 and M72 by PEBP1, a dose-response curve was performed in HEK cells expressing P2 and M72 and loaded with fura-2. The results confirmed P2 as a responsive receptor, with maximum response amplitude at 0.02 μg/μL PEBP1 concentration (Figure S6), and M72 as a non-responsive receptor to PEBP1. In fact, HEK cells expressing M72 exhibited no Ca^{2+} response at all tested concentrations of PEBP1 (Figure S6). Consistent with these results, we found that P2 and M72 glomeruli are located in distinct areas of the OB with high (medial side; P2) and low (posterior side; M72) expression of PEBP1, respectively (Figure S7). In wild-type mice, mature glomeruli are innervated exclusively by fibers expressing the same OR (Mombaerts et al., 1996; Ressler et al., 1994; Vassar et al., 1994). Convergence of OSN axons was analyzed in horizontal bulb sections of mice obtained by crossing PEBP1$^{-/-}$ and P2-GFP mice and PEBP1$^{-/-}$ and M72-YFP, using antibodies against olfactory marker protein (OMP), a marker for mature OSNs, to label the glomeruli of all ORs (Danciger et al., 1989). In P2-GFP and in P2-GFP; PEBP1$^{+/-}$ mice, P2-GFP-positive neurites targeted glomeruli formed by fibers positive for both OMP and GFP (e.g., expressing P2), resulting in a "P2-homogeneous glomerulus." However, in P2-GFP; PEBP1$^{+/-}$ mice, P2-GFP-expressing axons targeted additional OMP-positive, GFP-negative glomeruli, indicating the formation of heterogeneous glomeruli (Figure 6). In homozygous null PEBP1 mice (e.g., P2-GFP; PEBP1$^{-/-}$ mice), P2 axons innervated a significantly higher number of heterogeneous glomeruli with respect to control and heterozygous mice (Figures 6 and S8). The key feature of the olfactory map is the stereotyped position of each glomerulus in the OB. We analyzed whole-mount (Figures 7A–7D) and biochemically cleared whole OBs (Figures 7F and 7G; Videos S1 and S2) for the 2D and 3D location of the main P2 homogeneous glomeruli. The area of the lateral and medial surface of the OB, where P2 glomeruli are located, was similar in control, P2-GFP; PEBP1$^{+/-}$, and P2-GFP; PEBP1$^{-/-}$ mice (Figure 7E). The position along the dorso-ventral (D-V) axis of P2 glomeruli was unaffected in control mice with respect to mutant mice. However, P2-GFP; PEBP1$^{-/-}$ mice exhibited a significant shift of both the primary lateral and medial P2 glomeruli along the antero-posterior (A-P) axis with the lateral glomerulus shifted toward the posterior and the medial glomerulus shifted toward the anterior in both whole mounts and cleared whole bulbs of P2-GFP; PEBP1$^{-/-}$ mice when compared with control animals (Figures 7H and 7I).

In M72-YFP; PEBP1$^{+/-}$ and in M72-YFP; PEBP1$^{-/-}$ mice, M72-YFP axons converge to form homogeneous glomeruli (e.g., formed by fibers positive for OMP and YFP; Figures 6D–6Z) in the proper location as in control M72-YFP mice (Figures S8G–S8K). These results indicate that the interaction between PEBP1 and the responsive OR, such as P2, is required for the

stimulation period are indicated by traces in shades of gray. Black arrows indicate the pipette position. OSNs were stimulated with pulsatile application of (A) Ringer's solution, (B) forskolin (FRSK), (C) odors mixture, (D) IEC-2, and (E) PEBP1. Scale bar, 20 μm.

(F) Distribution of turning angles for all neurons in response to the tested stimuli

(G) Summary of results, reported as mean ± SEM.

(H) Turning angles (°), in response to different stimuli, reported as mean ± SEM. One-way ANOVA; Bonferroni corrected; *$p < 0.05$; **$p < 0.01$; ***$p < 0.001$. See also Figure S3.

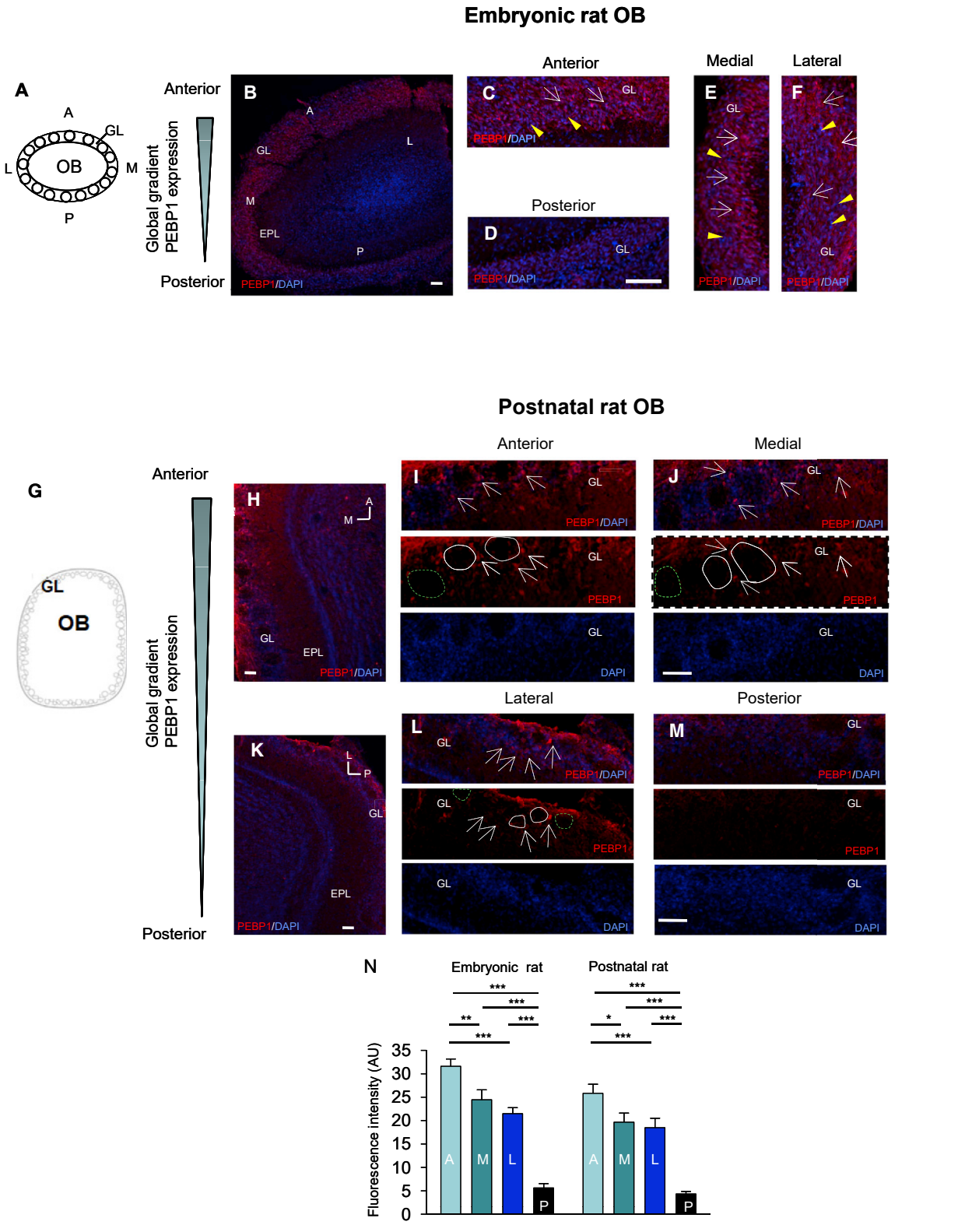

(legend on next page)

proper targeting of OSN axons to the specific target glomeruli in the OB. PEBP1 does not affect the spatial location and the convergence of M72-expressing fibers (Figure S8), in agreement with our *in vitro* data (Figures 2H, 2I, and S6) that indicated ORM72 as non-responsive to PEBP1.

DISCUSSION

In the present study, we provide evidence that the ORs expressed at the axon terminal direct the targeting of sensory neurons mediated by cues expressed in the OB. Among these cues, we identified PEBP1 as one of the putative ligands. We identified this unexpected ligand using an unbiased approach, characterizing a protein extract from the OB that was able to stimulate a local Ca^{2+} response when applied to the axon terminal of OSN. This classical readout of OR activation (Bozza and Kauer, 1998; Imai et al., 2006; Malnic et al., 1999) has previously only been used to identify odor ligands for an OR. When adenylyl cyclase is pharmacologically blocked, the Ca^{2+} response is abolished as one would expect for an OR-mediated response. A further support that the Ca^{2+} response was due to OR activation was obtained by transfecting HEK cells with specific ORs and demonstrating response to stimulus in comparison to HEK cells lacking the specific ORs did not exhibit Ca^{2+} response to the same stimulating molecules. The physiological relevance was deduced from the fact that the OB molecules were able to modulate the axon turning behavior of sensory axons *in vitro*, corroborating their function as axon guidance molecules. Notably, OSN axons exhibit attractive and repulsive behaviors in response to a gradient of the same cue (Figure 3F). These results can be explained by the fact that the turning behavior was performed on embryonic rat OSNs, whose OR identity was unknown. Our data indicate that cues elaborated in the OB, such as IEC-2 and PEBP1, can activate specific subsets of ORs. Therefore, depending on the type of OR expressed on the axon terminal, the same guidance molecule can elicit attractive or repulsive behavior in different OSNs expressing different ORs (see Figures 3 and S3).

Mass spectrometry of the active pool of molecules from the OB identified PEBP1 as a putative ligand of the axonal OR. PEBP1 is a highly conserved cytoplasmic protein of ~21 kDa that can be secreted via a non-classic pathway. The small molecular weight of PEBP1, ability of it to be secreted, ability to modulate G-protein coupled receptors (e.g., the adrenergic receptor; Goumon et al., 2004; Granovsky and Rosner, 2008), and the presence of olfactory deficits in mice carrying a PEBP1-null mutation (Theroux et al., 2007) make PEBP1 a prime candidate for this role.

Our data support that PEBP1 activates a specific set of ORs expressed at the OSN axon terminal to regulate axon turning behavior of sensory neurons. Although these results suggest a direct ligand-receptor interaction that leads to activation of the axonal OR, we cannot rule out the possibility of indirect activation due to the absence of a reliable assay that demonstrates the direct binding of PEBP1 to an OR. Among the ORs tested, M72 was not responsive to PEBP1, suggesting the potential for additional ligands for regulating the axon guidance of other subsets of ORs.

The *in vivo* physiological relevance of our findings is corroborated by the fact that mice carrying a null mutation of PEBP1 exhibit a perturbed sensory map. In OBs devoid of PEBP1 ($PEBP1^{-/-}$), the targeting of P2-expressing axons and the localization of the corresponding glomeruli were altered. P2-expressing OSN axons form not only the main P2 homogeneous glomeruli but also innervate non-target glomeruli, leading to the formation of heterogeneous glomeruli that violate the canonical one-OR one glomerulus rule. The locations of the main P2 glomeruli were also significantly shifted along the A-P axis in mice deficient in PEBP1 in respect to controls. Together, these findings suggest that molecules residing in the OB, such as PEBP1, activate the axonal OR and provide neurons with guidance cues critical for reaching the proper target area.

In contrast to P2 axons, the convergence of M72 axons and the location of the corresponding glomeruli were unaltered in PEBP1-deficient mice. This finding is in concordance with the M72 receptors lack of responsiveness to PEBP1 in *in vitro*

Figure 4. Expression of PEBP1 in Rat OB

(A) Schematic representation of embryonic rat OB.

(B) Low-magnification image of a coronal section of the rat OB labeled for PEBP1 (red). Nuclear marker DAPI (blue) is shown. High expression of PEBP1 is detected in periglomerular cells in the anterior, medial, and lateral side of embryonic rat OB. Low expression is present in the posterior side. Rat embryos, n = 5, from 4 pregnant rats. Scale bar, 50 μm.

(C–F) Higher magnification images of the anterior (C), posterior (D), medial (E), and lateral (F) areas related to the section shown in (B). Scale bar, 100 μm.

(G) Schematic representation of postnatal rat OB.

(H) Low-magnification image of the antero-medial portion of the OB in postnatal rat (postnatal day 2 [P2]), labeled for PEBP1 (red) and DAPI (blue). Scale bar, 50 μm.

(I and J) Higher magnification of the anterior (I) and medial (J) sides of the section in (H), where high expression of PEBP1 can be observed in periglomerular cells. Scale bar, 100 μm.

(K) Image of the lateral and posterior side of the OB of postnatal rat (P2), labeled for PEBP1 (red) and DAPI (blue). Scale bar, 50 μm.

(L and M) Higher magnification of the lateral and posterior areas of the section in (K). PEBP1 labeling is observed around the glomeruli, in the periglomerular cells, and in the lateral aspect of the OB in (L). Low expression of PEBP1 is detected in the posterior side in (M). Postnatal rat pups, P0–P4, n = 5, from 5 litters. Scale bar, 100 μm.

(N) Quantification of PEBP1 expression in the OB in embryonic and postnatal rats. Bars represent SEM. One-way ANOVA; Bonferroni corrected; *$p < 0.05$; **$p < 0.01$; ***$p < 0.001$.

Arrows indicate PEBP1-positive cells. Yellow arrowheads and dashed green circles indicate glomeruli surrounded by low expression of PEBP1. Solid circles indicate glomeruli surrounded by high expression of PEBP1. White arrows indicate periglomerular cells expressing high level of PEBP1. A, anterior; EPL, external plexiform layer; GL, glomerular layer; L, lateral; M, medial; p, posterior.

See also Figures S4, S5, and S7.

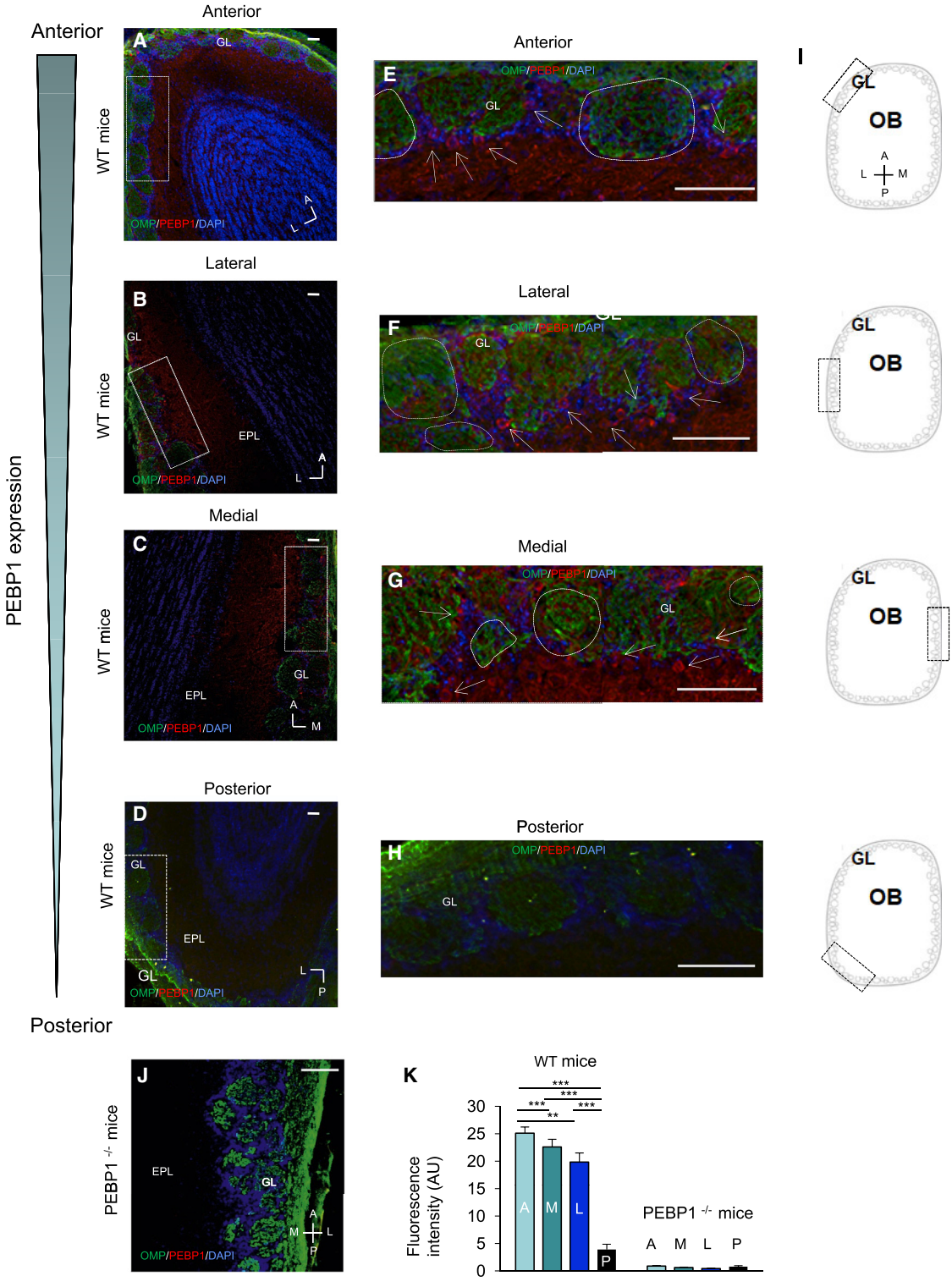

Figure 5. Expression of PEBP1 in Mouse OB

Coronal sections of the mouse OB (>P40) labeled for PEBP1 (red), OMP (green), and nuclear marker DAPI (blue).

(A–D) PEBP1 is highly expressed in periglomerular cells along the anterior (A), lateral (B), and medial (C) side of the OB. PEBP1 expression is barely detected in the posterior (D) side. Scale bars, 50 μm.

(legend continued on next page)

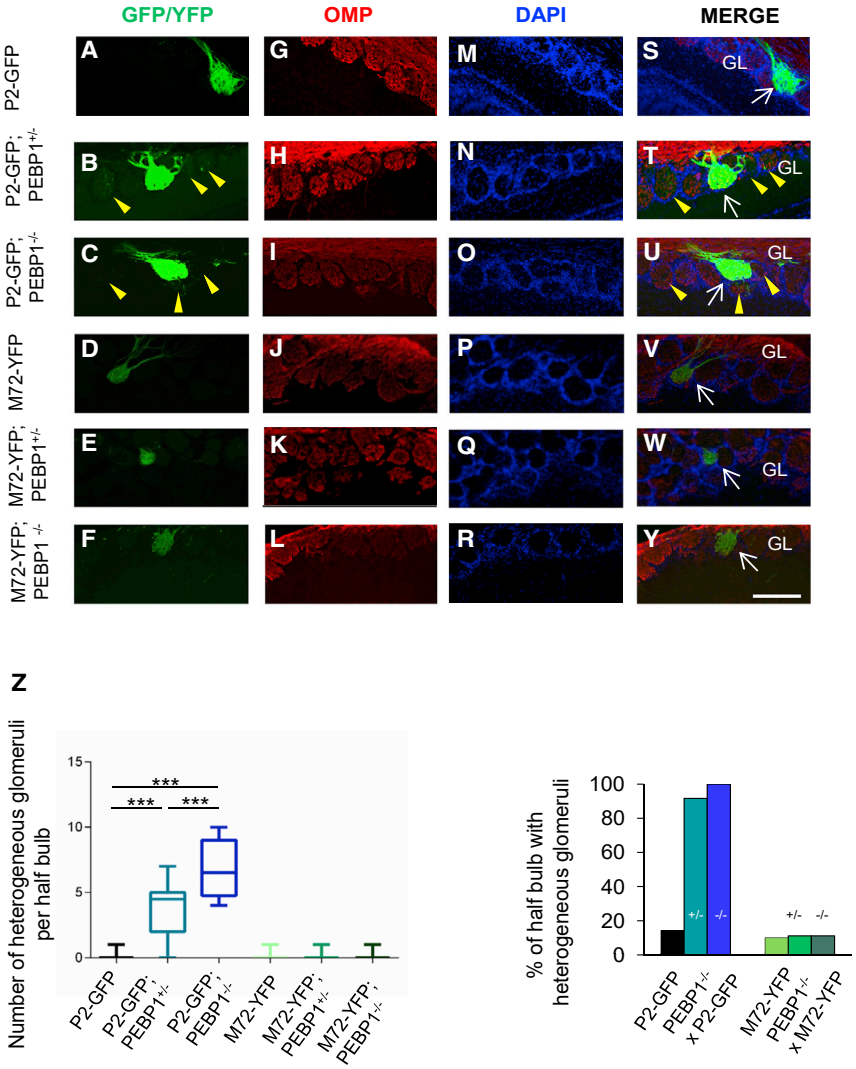

Figure 6. Organization of Glomeruli in Control and PEBP1 Mutant Mice

(A–Y) Organization of P2 and M72 glomeruli (GFP/YFP, green, A–F) revealed by immunolabeling sections of the OB with antibodies against OMP (red, G–L) and the nuclear marker DAPI (blue, M–R). Merged images are shown (S–Y). P2 axons positive for GFP and OMP coalesce to form a main homogeneous glomerulus in control P2-GFP (A and S; mice, n = 6; bulb, n = 7), in P2-GFP; PEBP1$^{+/-}$ (B and T; mice, n = 4; bulb, n = 8), and in P2-GFP; PEBP1$^{-/-}$ mice (C and U; mice, n = 6; bulb, n = 9). P2 axons innervate also adjacent glomeruli that result to be formed by fibers positive for GFP and OMP (e.g., expressing P2) but also by fibers positive only for OMP (e.g., expressing a different OR, heterogeneous glomeruli) in P2-GFP; PEPB1$^{+/-}$ (B and T) and in P2-GFP; PEPB1$^{-/-}$ mice (C and U). M72 glomeruli (D–F) are formed by OSN axons expressing YFP and positive for OMP (e.g., homogeneous glomeruli) in control M72-YFP (mice, n = 5; bulb, n = 5; D and V) and also in M72-YFP; PEPB1$^{+/-}$ (mice, n = 6; bulb, n = 9; E and W) and in M72-YFP; PEPB1$^{-/-}$ mice (mice, n = 6; bulb, n = 9; F and Y). Scale bar, 100 μm. White arrows indicate homogeneous glomeruli. Yellow arrowheads indicate heterogeneous glomeruli.

(Z) Summary of results. One-way ANOVA; Bonferroni corrected; ***p < 0.001.

See also Figure S8.

location of olfactory glomeruli along the A-P axis, exhibits a global gradient along the A-P axis and a patchy distribution at the glomerular level (Assens et al., 2016; Col et al., 2007; Zapiec et al., 2016).

Periglomerular cells are a highly suitable location for the expression of guidance cues that direct the incoming axons, such as PEBP1. The role of postsynaptic cells in the formation of the sensory map is corroborated by previous works (Cutforth et al., 2003; Scolnick et al., 2008), in which the interaction between cues elaborated in periglomerular and mitral cells (such as Eph and IGF1) and in OSNs (ephrin and IGF1 R) was reported to direct OSN axons to their final target. On the other hand, previous data indicated that the postsynaptic cells are dispensable for the coalescence of like fibers to form glomeruli. Indeed, in the double knockout (KO) of Dlx1/Dl2, in which periglomerular cells are absent, and of Tbr1/Tbr2, devoid of most of mitral and tufted cells (Bulfone et al., 1998), the convergence of like axons to form the main glomeruli seems to occur. However, it has to be considered that the double Dlx1/2 KO die within a

experiments and suggests that other ligands for the axonal ORs remain unidentified.

The different impact of PEBP1 on P2 and M72 glomeruli is reflected by the different distribution of PEBP1 in the OB. The ligand is highly expressed in the periglomerular cells in the antero-lateral and the antero-medial wall, where P2 glomeruli are located, but it is hardly detected in the posterior part of the OB, where M72 fibers converge to form glomeruli. This expression pattern results in a global gradient of PEBP1 along the A-P axis. However, at the local level, glomeruli surrounded by high PEBP1 expression are intermingled to glomeruli with very low PEBP1 labeling. In a similar way, neuropilin-1, a molecule involved in modulating the

(E–H) Higher magnification of the areas in the dashed rectangles in (A)–(D), respectively. (E) is the higher magnification of (A), (F) of (B), (G) of (C), and (H) of (D).White arrows indicate PEBP1-positive periglomerular cells. Dashed circles indicate glomeruli surrounded by low expression of PEBP1. Scale bars, 100 μm.

(I) Schematic of mouse OB. Dashed rectangles indicate the position of the area included in dashed rectangles in (A)–(D) in the whole OB.

(J) Staining for PEBP1 in coronal sections of the OB of PEBP1$^{-/-}$ mice. PEBP1-positive cells are not present in the OB of PEBP1$^{-/-}$ mice. Scale bar, 100 μm.

(K) Quantification of PEBP1 expression in the OB of wild-type (WT) (n = 8) and PEBP1$^{-/-}$ (n = 4) mice. Bars represent SEM. One-way ANOVA; Bonferroni corrected; one-way *p < 0.05; **p < 0.01; ***p < 0.001.

See also Figures S4, S5, and S7.

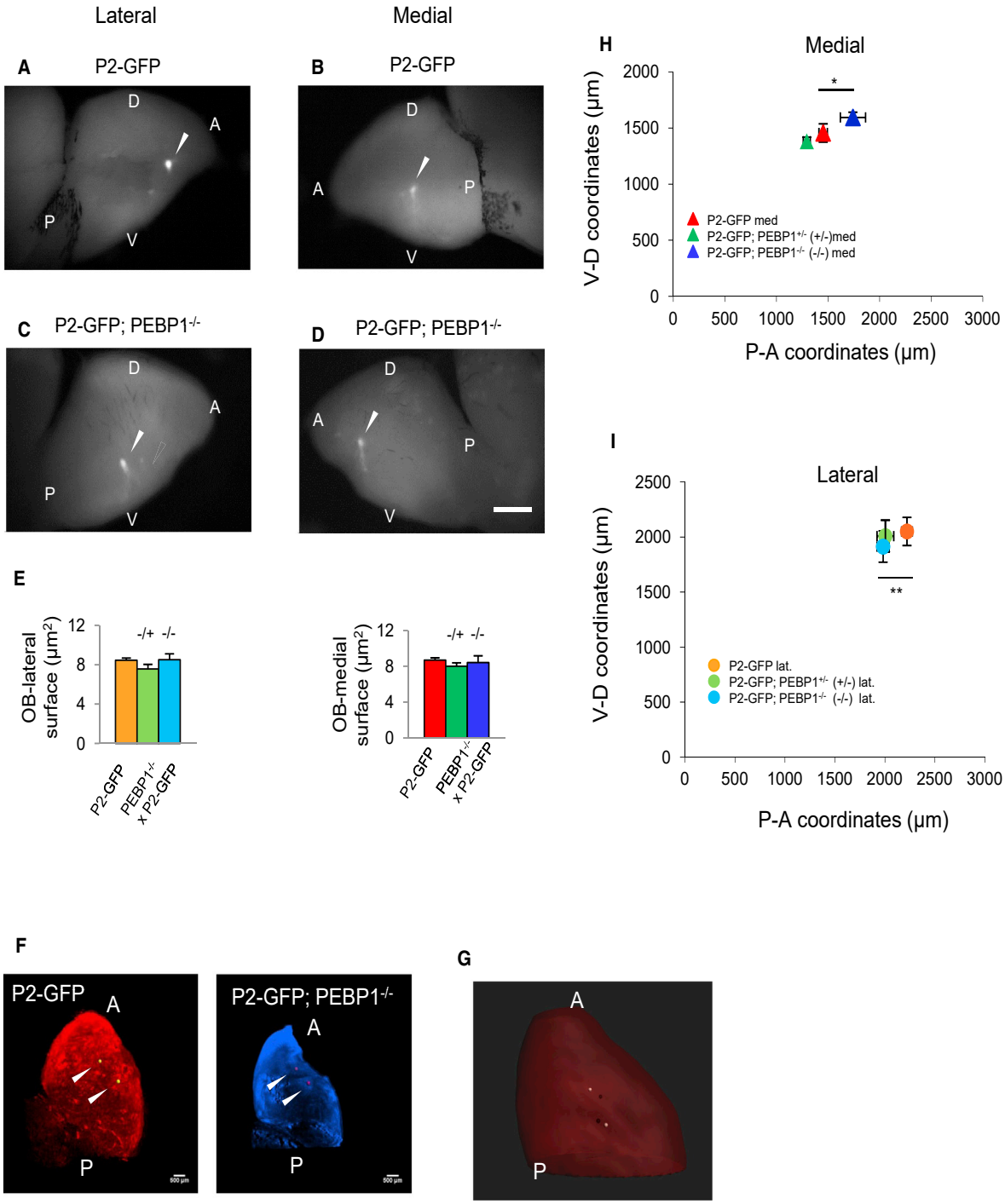

Figure 7. Altered Location of P2-GFP Glomeruli in PEBP1 Mutant Mice

(A–D) Whole mount view of the lateral (A and C) and medial (B and D) aspect of the OB in control P2-GFP mice (A and B) and in P2-GFP; PEBP1$^{-/-}$ mice (C and D). P2-GFP-expressing fibers converge to form the main glomerulus on the lateral and on the medial surface of the OB. Scale bar, 1 mm.

(E) Areas of the lateral and the medial aspects of the OB in control P2-GFP, in P2-GFP; PEBP1$^{+/-}$, and in P2-GFP; PEBP1$^{-/-}$ mice, respectively. Bars represent SEM.

(F) Images of cleared whole bulbs of P2-GFP control (left) and in P2-GFP; PEBP1$^{-/-}$ (right) mice. The position of the medial and lateral glomeruli is represented by yellow and red dots in P2 -GFP and in P2-GFP; PEBP1$^{-/-}$ mice, respectively. Scale bars, 500 µm.

(G) Visualization of the average position of the glomeruli displayed in relation to a representative cleared whole bulb. Pink and black dots indicate the mean location of the medial and the lateral glomeruli, respectively, in P2-GFP (pink) and in P2-GFP; PEBP1$^{-/-}$ (black) mice. Relative positions in the bulb are shown (normalized values without scale).

(legend continued on next page)

few hours after birth and exhibit striking hypoplastic bulbs. In this context, the exact location of the glomeruli, a key feature of the topographic map, cannot be ascertained, and it could be extremely challenging, if not impossible, to detect mistargeted fibers. All together, these data appear to indicate that the coalescence of like fibers to form glomeruli does not require postsynaptic cells, which are important for directing axon targeting and the unique location of glomeruli in the OB. This model recapitulates the mechanism underlying the formation of the topographic map in other sensory modalities, such as the visual system. The paired axon guidance cues neuropilin1-Sema3A, which are thought to contribute to defining the position of glomeruli along the A-P axis, appear as an exception to this model, because both are reported to be expressed by OSNs (Imai et al., 2009).

We observed that the position of P2 and M72 glomeruli along the D-V axis remains unaffected in PEBP1-deficient mice with respect to controls. This is consistent with the fact that the distribution along the D-V axis does not rely on the OR identity but reflects the location of OSNs in overlapping zones along the D-V axis of the epithelium instead (Miyamichi et al., 2005; Ressler et al., 1994; Vassar et al., 1994). Molecules such as Slit1, Robo2 (Cloutier et al., 2002, 2004; Nguyen-Ba-Charvet et al., 2008), neuropilin-2, and Sema3F (Cloutier et al., 2002; Takeuchi et al., 2010; Walz et al., 2002) contribute to the spatial distribution of sensory afferents along the D-V axis.

The observation that at least one OR (M72) is not responsive to PEBP1 suggests, as mentioned earlier, the presence of additional molecules, whose number and identity remain to be clarified. Two possibilities can be envisioned. First, the number of cues elaborated in the OB is the same as the OR number, such that there is a specific cue for each OR. This model would imply around eleven hundred possible cues with very specific and localized expression patterns. Second, there is a limited number of molecules that guide OSN axons to the right position. The data we obtained here with the putative ligand, PEBP1, are in accordance with the second model. Indeed, PEBP1 appears to be rather broadly expressed, suggesting that this putative ligand can interact with different subsets of ORs. This was confirmed by demonstrating that, in addition to P2, PEBP1 was also able to activate EG, Olfr62, and S6 receptors. Each receptor type exhibits, however, a different degree of response, suggesting different affinities for PEBP1. Thus, we favor a model where a small number of molecules expressed in gradients in the OB recognizes, with a different affinity, distinct subset of ORs, driving the OSN axons to a given OB area. At the local level, characterized by a patchy pattern of PEBP1 expression in nearby glomeruli, the distinct affinity of a given OR for PEBP1 will determine the location of the OSN axons convergence. The presence of a global, but not a continuous, gradient of PEBP1 along the A-P axis, along with the patchy expression of PEBP1 at the local glomerular level, could explain the shift in opposite directions of the medial and lateral glomeruli expressing P2 in PEBP1$^{-/-}$ mice. It is worth noting that, in wild-type control mice, the location of the medial and lateral glomeruli is not the same along the A-P axis. Therefore, each glomerulus is likely to be differentially affected by the patchy local distribution of PEBP1 along with other guidance cues and to shift in different directions in the absence of PEBP1. Alternatively, in the absence of PEBP1, glomeruli location could shift in a stochastic manner. The consistent anterior shift of the medial glomeruli and posterior shift of the later glomeruli seem to favor the former model.

Although the OR plays an instructive role in determining the glomerular location, it is not the only determinant (Wang et al., 1998). Noteworthy, the identity of the OR is highly correlated and can modulate the expression of other guidance and adhesion molecules, such as the level of ephrin-A proteins (Cutforth et al., 2003), Kirrel2 and 3 (Serizawa et al., 2006), Big 2 (Kaneko-Goto et al., 2008), and neuropilin-1, whose expression is regulated by OR-derived cAMP levels (Imai et al., 2006). The mechanism underlying the OR-derived cAMP rise remains elusive. Our data seem to complement these findings, suggesting that activation of the axonal OR by cues originating from the OB leads to a local increase of cAMP that, in turn, can regulate the expression of other guidance cues involved in olfactory map formation (Maritan et al., 2009; Pietrobon et al., 2011). Considering all of these elements, we favor a model in which the OR is expressed at the axon terminal along with other guidance cues. A unique combination of axon guidance molecules expressed at the axon terminal along with the OR will provide the OSN with information to reach a unique glomerular target in the OB. Adhesion molecules, such as Kirrel2 and 3 (Serizawa et al., 2006), Big2 (Kaneko-Goto et al., 2008), and cadherins (Mountoufaris et al., 2017), could refine the coalescence of sensory fibers once they reach the target area.

Our data resolve a long-standing paradox in the field. Although the olfactory map hinges on OR identity, several studies indicated that odor-evoked activity does not significantly affect the convergence of sensory axons (Belluscio et al., 1998; Lin et al., 2000; Zheng et al., 2000). On the other hand, spontaneous afferent activity was demonstrated to be required for the refined wiring and maintenance of the topographic map, although it does not instruct the spatial targeting of axons (Lorenzon et al., 2015; Yu et al., 2004). It is worth noticing that the OR identity regulates not only odor-evoked activity but also spontaneous firing in sensory neurons (Connelly et al., 2013; Reisert, 2010). It was therefore hypothesized that ligand-independent activation was the origin of the OR-derived cAMP, which is required to target sensory neurons to their glomeruli (Nakashima et al., 2013). The considerable variation of basal activity, even among OSNs expressing the same OR, makes it unclear how specificity of targeting could be achieved in this context. Our work here, after more than 20 years from the identification of the OR's role in the formation of the sensory map, unveils the identity of a putative ligand of the axonal ORs. The distinct activation mechanisms

(H and I) Localization of P2-GFP medial (H) and lateral (I) glomeruli along the ventro-dorsal (V-D) and the postero-anterior (P-A) axis of the OB in P2-GFP control (mice, n = 10; bulb, n = 18), P2-GFP; PEBP1$^{+/-}$ mice (mice, n = 5; bulb, n = 9), and in P2-GFP; PEBP1$^{-/-}$ mice (mice, n = 8; bulb, n = 14). P2 glomeruli location along the A-P axis of the OB is significantly shifted in P2-GFP; PEBP1$^{-/-}$ mice in respect to controls. Bars represent SEM. Analysis of P2-GFP glomeruli location along the A-P axis; one-way ANOVA; Bonferroni corrected; *$p < 0.05$; **$p < 0.01$.
Arrowheads indicate glomeruli. V, ventral.
See also Figure S8 and Videos S1 and S2.

for ORs expressed at the opposite poles of OSNs, by odors at the dendrite and by OB-originating cues at the axon terminal, explain the dual function of these receptors, linking specificity of odor perception to its internal representation as a topographic sensory map. Our model proposes that the sensory axons "sniff" their way through the OB to reach their target glomerulus.

STAR★METHODS

Detailed methods are provided in the online version of this paper and include the following:

- KEY RESOURCES TABLE
- LEAD CONTACT AND MATERIALS AVAILABILITY
- EXPERIMENTAL MODEL AND SUBJECT DETAILS
  - Animals
  - Primary culture of rat and mouse olfactory sensory neurons
  - HEK293T cell culture
- METHOD DETAILS
  - Isolation of olfactory bulb products
  - Identification of the eluted material from HPLC
  - Ca^{2+} imaging in olfactory sensory neurons and HEK293T cells
  - Cyclic AMP imaging in olfactory sensory neurons
  - Stimuli
  - Time-lapse imaging of axon turning of rat olfactory sensory neurons
  - Expression and purification of pGEX-RKIP-1 fusion protein
  - RT-PCR
  - Western blot
  - Immunohistochemistry
  - Measurements of glomeruli position in the olfactory bulb
- QUANTIFICATION AND STATISTICAL ANALYSIS
  - Statistical tests, sample size, and P values are listed in each figure legend
- DATA AND CODE AVAILABILITY

SUPPLEMENTAL INFORMATION

Supplemental Information can be found online at https://doi.org/10.1016/j.celrep.2019.11.099.

ACKNOWLEDGMENTS

We are grateful to J.A. Gogos for advice and for generously providing the P2-GFP mice. We thank Evan Keller for PEPB1$^{-/-}$ mice and M. Rosner for pGEX2T-rat-RKIPcDNA. We thank C. Fecchio and G. Lolli for helping with chromatography experiments. We thank Dorien Vandael and Frank Vernaillen for helping with the clearing experiments. We are grateful to Kevin Zhu and Priyanka Meesa for their contribution in editing the manuscript. We thank all members of Lodovichi lab for support and insightful discussion. This work was supported by Armenise-Harvard Foundation CDA (USA), Telethon Foundation (Italy) GGP13187, GGP 11116 and GGP19281, Cariparo Foundation grant (Italy), and MIUR-CNR Nanomax (Italy) to C.L.

AUTHOR CONTRIBUTIONS

I.Z. and S.F. performed imaging experiments and data analysis; S.A.F. contributed to imaging experiments and data analysis; S.F. and N.R. performed experiments and analysis on organization of glomeruli; S.F. performed immunofluorescence, RT-PCR, and western blots; E.C. contributed to the production of PEBP1; R.B. performed SEC and IEC; P.P.d.L. performed RPC and mass spectrometry; A.K. and S.M. performed clarity on whole bulb and related analysis; Y.F. and H.M. performed quantification assay for cell population, dose response curve, and EC_{50}; C.L. designed the project, supervised experiments, and performed data analysis; B.D.S. and C.L. wrote the first version of the paper; and H.M. and C.L. wrote the final version of the paper.

DECLARATION OF INTERESTS

The authors declare no competing interests.

Received: September 27, 2017
Revised: August 26, 2019
Accepted: November 21, 2019
Published: December 24, 2019

REFERENCES

Al-Mulla, F., Bitar, M.S., Taqi, Z., and Yeung, K.C. (2013). RKIP: much more than Raf kinase inhibitory protein. J. Cell. Physiol. *228*, 1688–1702.

Assens, A., Dal Col, J.A., Njoku, A., Dietschi, Q., Kan, C., Feinstein, P., Carleton, A., and Rodriguez, I. (2016). Alteration of Nrp1 signaling at different stages of olfactory neuron maturation promotes glomerular shifts along distinct axes in the olfactory bulb. Development *143*, 3817–3825.

Barnea, G., O'Donnell, S., Mancia, F., Sun, X., Nemes, A., Mendelsohn, M., and Axel, R. (2004). Odorant receptors on axon termini in the brain. Science *304*, 1468.

Belluscio, L., Gold, G.H., Nemes, A., and Axel, R. (1998). Mice deficient in G(olf) are anosmic. Neuron *20*, 69–81.

Bozza, T.C., and Kauer, J.S. (1998). Odorant response properties of convergent olfactory receptor neurons. J. Neurosci. *18*, 4560–4569.

Bradley, J., Reisert, J., and Frings, S. (2005). Regulation of cyclic nucleotide-gated channels. Curr. Opin. Neurobiol. *15*, 343–349.

Buck, L., and Axel, R. (1991). A novel multigene family may encode odorant receptors: a molecular basis for odor recognition. Cell *65*, 175–187.

Bulfone, A., Wang, F., Hevner, R., Anderson, S., Cutforth, T., Chen, S., Meneses, J., Pedersen, R., Axel, R., and Rubenstein, J.L. (1998). An olfactory sensory map develops in the absence of normal projection neurons or GABAergic interneurons. Neuron *21*, 1273–1282.

Chesler, A.T., Zou, D.J., Le Pichon, C.E., Peterlin, Z.A., Matthews, G.A., Pei, X., Miller, M.C., and Firestein, S. (2007). A G protein/cAMP signal cascade is required for axonal convergence into olfactory glomeruli. Proc. Natl. Acad. Sci. USA *104*, 1039–1044.

Cloutier, J.F., Giger, R.J., Koentges, G., Dulac, C., Kolodkin, A.L., and Ginty, D.D. (2002). Neuropilin-2 mediates axonal fasciculation, zonal segregation, but not axonal convergence, of primary accessory olfactory neurons. Neuron *33*, 877–892.

Cloutier, J.F., Sahay, A., Chang, E.C., Tessier-Lavigne, M., Dulac, C., Kolodkin, A.L., and Ginty, D.D. (2004). Differential requirements for semaphorin 3F and Slit-1 in axonal targeting, fasciculation, and segregation of olfactory sensory neuron projections. J. Neurosci. *24*, 9087–9096.

Col, J.A., Matsuo, T., Storm, D.R., and Rodriguez, I. (2007). Adenylyl cyclase-dependent axonal targeting in the olfactory system. Development *134*, 2481–2489.

Connelly, T., Savigner, A., and Ma, M. (2013). Spontaneous and sensory-evoked activity in mouse olfactory sensory neurons with defined odorant receptors. J. Neurophysiol. *110*, 55–62.

Cutforth, T., Moring, L., Mendelsohn, M., Nemes, A., Shah, N.M., Kim, M.M., Frisén, J., and Axel, R. (2003). Axonal ephrin-As and odorant receptors: coordinate determination of the olfactory sensory map. Cell *114*, 311–322.

Danciger, E., Mettling, C., Vidal, M., Morris, R., and Margolis, F. (1989). Olfactory marker protein gene: its structure and olfactory neuron-specific expression in transgenic mice. Proc. Natl. Acad. Sci. USA *86*, 8565–8569.

Dubacq, C., Jamet, S., and Trembleau, A. (2009). Evidence for developmentally regulated local translation of odorant receptor mRNAs in the axons of olfactory sensory neurons. J. Neurosci. *29*, 10184–10190.

Feinstein, P., Bozza, T., Rodriguez, I., Vassalli, A., and Mombaerts, P. (2004). Axon guidance of mouse olfactory sensory neurons by odorant receptors and the beta2 adrenergic receptor. Cell *117*, 833–846.

Frayne, J., Ingram, C., Love, S., and Hall, L. (1999). Localisation of phosphatidylethanolamine-binding protein in the brain and other tissues of the rat. Cell Tissue Res. *298*, 415–423.

Gogos, J.A., Osborne, J., Nemes, A., Mendelsohn, M., and Axel, R. (2000). Genetic ablation and restoration of the olfactory topographic map. Cell *103*, 609–620.

Goumon, Y., Angelone, T., Schoentgen, F., Chasserot-Golaz, S., Almas, B., Fukami, M.M., Langley, K., Welters, I.D., Tota, B., Aunis, D., and Metz-Boutigue, M.H. (2004). The hippocampal cholinergic neurostimulating peptide, the N-terminal fragment of the secreted phosphatidylethanolamine-binding protein, possesses a new biological activity on cardiac physiology. J. Biol. Chem. *279*, 13054–13064.

Granovsky, A.E., and Rosner, M.R. (2008). Raf kinase inhibitory protein: a signal transduction modulator and metastasis suppressor. Cell Res. *18*, 452–457.

Harper, S., and Speicher, D.W. (2011). Purification of proteins fused to glutathione S-transferase. Methods Mol. Biol. *681*, 259–280.

Imai, T., Suzuki, M., and Sakano, H. (2006). Odorant receptor-derived cAMP signals direct axonal targeting. Science *314*, 657–661.

Imai, T., Yamazaki, T., Kobayakawa, R., Kobayakawa, K., Abe, T., Suzuki, M., and Sakano, H. (2009). Pre-target axon sorting establishes the neural map topography. Science *325*, 585–590.

Kaneko-Goto, T., Yoshihara, S., Miyazaki, H., and Yoshihara, Y. (2008). BIG-2 mediates olfactory axon convergence to target glomeruli. Neuron *57*, 834–846.

Kerstens, A., Corthout, N., Pavie, B., Huang, Z., Vernaillen, F., Vande Velde, G., and Munck, S. (2019). A label-free multicolor optical surface tomography (ALMOST) imaging method for nontransparent 3D samples. BMC Biol. *17*, 1.

Lin, D.M., Wang, F., Lowe, G., Gold, G.H., Axel, R., Ngai, J., and Brunet, L. (2000). Formation of precise connections in the olfactory bulb occurs in the absence of odorant-evoked neuronal activity. Neuron *26*, 69–80.

Lodovichi, C., and Belluscio, L. (2012). Odorant receptors in the formation of the olfactory bulb circuitry. Physiology (Bethesda) *27*, 200–212.

Lohof, A.M., Quillan, M., Dan, Y., and Poo, M.M. (1992). Asymmetric modulation of cytosolic cAMP activity induces growth cone turning. J. Neurosci. *12*, 1253–1261.

Lorenzon, P., Redolfi, N., Podolsky, M.J., Zamparo, I., Franchi, S.A., Pietra, G., Boccaccio, A., Menini, A., Murthy, V.N., and Lodovichi, C. (2015). Circuit formation and function in the olfactory bulb of mice with reduced spontaneous afferent activity. J. Neurosci. *35*, 146–160.

Malnic, B., Hirono, J., Sato, T., and Buck, L.B. (1999). Combinatorial receptor codes for odors. Cell *96*, 713–723.

Maritan, M., Monaco, G., Zamparo, I., Zaccolo, M., Pozzan, T., and Lodovichi, C. (2009). Odorant receptors at the growth cone are coupled to localized cAMP and Ca2+ increases. Proc. Natl. Acad. Sci. USA *106*, 3537–3542.

Menini, A. (1999). Calcium signalling and regulation in olfactory neurons. Curr. Opin. Neurobiol. *9*, 419–426.

Miyamichi, K., Serizawa, S., Kimura, H.M., and Sakano, H. (2005). Continuous and overlapping expression domains of odorant receptor genes in the olfactory epithelium determine the dorsal/ventral positioning of glomeruli in the olfactory bulb. J. Neurosci. *25*, 3586–3592.

Mombaerts, P., Wang, F., Dulac, C., Chao, S.K., Nemes, A., Mendelsohn, M., Edmondson, J., and Axel, R. (1996). Visualizing an olfactory sensory map. Cell *87*, 675–686.

Mountoufaris, G., Chen, W.V., Hirabayashi, Y., O'Keeffe, S., Chevee, M., Nwakeze, C.L., Polleux, F., and Maniatis, T. (2017). Multicluster Pcdh diversity is required for mouse olfactory neural circuit assembly. Science *356*, 411–414.

Nakashima, A., Takeuchi, H., Imai, T., Saito, H., Kiyonari, H., Abe, T., Chen, M., Weinstein, L.S., Yu, C.R., Storm, D.R., et al. (2013). Agonist-independent GPCR activity regulates anterior-posterior targeting of olfactory sensory neurons. Cell *154*, 1314–1325.

Nguyen-Ba-Charvet, K.T., Di Meglio, T., Fouquet, C., and Chédotal, A. (2008). Robos and slits control the pathfinding and targeting of mouse olfactory sensory axons. J. Neurosci. *28*, 4244–4249.

Pietrobon, M., Zamparo, I., Maritan, M., Franchi, S.A., Pozzan, T., and Lodovichi, C. (2011). Interplay among cGMP, cAMP, and Ca2+ in living olfactory sensory neurons in vitro and in vivo. J. Neurosci. *31*, 8395–8405.

Ponsioen, B., Zhao, J., Riedl, J., Zwartkruis, F., van der Krogt, G., Zaccolo, M., Moolenaar, W.H., Bos, J.L., and Jalink, K. (2004). Detecting cAMP-induced Epac activation by fluorescence resonance energy transfer: Epac as a novel cAMP indicator. EMBO Rep. *5*, 1176–1180.

Reisert, J. (2010). Origin of basal activity in mammalian olfactory receptor neurons. J. Gen. Physiol. *136*, 529–540.

Ressler, K.J., Sullivan, S.L., and Buck, L.B. (1994). A molecular dissection of spatial patterning in the olfactory system. Curr. Opin. Neurobiol. *4*, 588–596.

Schindelin, J., Arganda-Carreras, I., Frise, E., Kaynig, V., Longair, M., Pietzsch, T., Preibisch, S., Rueden, C., Saalfeld, S., Schmid, B., et al. (2012). Fiji: an open-source platform for biological-image analysis. Nat. Methods *9*, 676–682.

Scolnick, J.A., Cui, K., Duggan, C.D., Xuan, S., Yuan, X.B., Efstratiadis, A., and Ngai, J. (2008). Role of IGF signaling in olfactory sensory map formation and axon guidance. Neuron *57*, 847–857.

Serizawa, S., Miyamichi, K., Takeuchi, H., Yamagishi, Y., Suzuki, M., and Sakano, H. (2006). A neuronal identity code for the odorant receptor-specific and activity-dependent axon sorting. Cell *127*, 1057–1069.

Sharpe, J., Ahlgren, U., Perry, P., Hill, B., Ross, A., Hecksher-Sørensen, J., Baldock, R., and Davidson, D. (2002). Optical projection tomography as a tool for 3D microscopy and gene expression studies. Science *296*, 541–545.

Song, H.J., Ming, G.L., and Poo, M.M. (1997). cAMP-induced switching in turning direction of nerve growth cones. Nature *388*, 275–279.

Strotmann, J., Levai, O., Fleischer, J., Schwarzenbacher, K., and Breer, H. (2004). Olfactory receptor proteins in axonal processes of chemosensory neurons. J. Neurosci. *24*, 7754–7761.

Susaki, E.A., Tainaka, K., Perrin, D., Yukinaga, H., Kuno, A., and Ueda, H.R. (2015). Advanced CUBIC protocols for whole-brain and whole-body clearing and imaging. Nat. Protoc. *10*, 1709–1727.

Takeuchi, H., Inokuchi, K., Aoki, M., Suto, F., Tsuboi, A., Matsuda, I., Suzuki, M., Aiba, A., Serizawa, S., Yoshihara, Y., et al. (2010). Sequential arrival and graded secretion of Sema3F by olfactory neuron axons specify map topography at the bulb. Cell *141*, 1056–1067.

Theroux, S., Pereira, M., Casten, K.S., Burwell, R.D., Yeung, K.C., Sedivy, J.M., and Klysik, J. (2007). Raf kinase inhibitory protein knockout mice: expression in the brain and olfaction deficit. Brain Res. Bull. *71*, 559–567.

Vassar, R., Chao, S.K., Sitcheran, R., Nuñez, J.M., Vosshall, L.B., and Axel, R. (1994). Topographic organization of sensory projections to the olfactory bulb. Cell *79*, 981–991.

Walz, A., Rodriguez, I., and Mombaerts, P. (2002). Aberrant sensory innervation of the olfactory bulb in neuropilin-2 mutant mice. J. Neurosci. *22*, 4025–4035.

Wang, F., Nemes, A., Mendelsohn, M., and Axel, R. (1998). Odorant receptors govern the formation of a precise topographic map. Cell *93*, 47–60.

Yu, C.R., Power, J., Barnea, G., O'Donnell, S., Brown, H.E., Osborne, J., Axel, R., and Gogos, J.A. (2004). Spontaneous neural activity is required for the establishment and maintenance of the olfactory sensory map. Neuron *42*, 553–566.

Zapiec, B., Bressel, O.C., Khan, M., Walz, A., and Mombaerts, P. (2016). Neuropilin-1 and the positions of glomeruli in the mouse olfactory bulb. eNeuro *3*, ENEURO.0123-16.2016.

Zheng, J.Q., and Poo, M.M. (2007). Calcium signaling in neuronal motility. Annu. Rev. Cell Dev. Biol. *23*, 375–404.

Zheng, C., Feinstein, P., Bozza, T., Rodriguez, I., and Mombaerts, P. (2000). Peripheral olfactory projections are differentially affected in mice deficient in a cyclic nucleotide-gated channel subunit. Neuron *26*, 81–91.

Zhuang, H., and Matsunami, H. (2007). Synergism of accessory factors in functional expression of mammalian odorant receptors. J. Biol. Chem. *282*, 15284–15293.

STAR★METHODS

KEY RESOURCES TABLE

REAGENT or RESOURCE	SOURCE	IDENTIFIER
Antibodies		
Rabbit-polyclonal anti-RKIP (PEBP1)	Millipore	Cat#07-137; RRID: AB_310389
Goat anti-Olfactory Marker Protein (OMP)	Wako Chemicals	Cat#544-10001; RRID: AB_664696
Alexa 488-conjugated Donkey anti-goat IgG (H+L)	JacksonImmuno	Cat#705-545-147; RRID:AB_2336933
Cy3-conjugated Donkey anti-rabbit IgG(H+L)	JacksonImmuno	Cat#711-165-152; RRID:AB_2307443
Cy3 conjugated Donkey anti-goat IgG (H+L)	JacksonImmuno	Cat#705-165-147; RRID:AB_2307351
Mouse-monoclonal anti-β-actin	Life Technologies	Cat#MA1-140; RRID:AB_2536844
Donkey Anti-Rabbit IgG ECL ™ Antibody, HRP Conjugated	GE Healthcare	Cat#NA9340; RRID:AB_772191
Sheep anti-mouse IgG ECL ™ Antibody, HRP Conjugated	GE Healthcare	Cat#NA931; RRID:AB_772210
Chemicals, Peptides, and Recombinant Proteins		
(±) Citronellal	Sigma Aldrich	Cat#C25-13
(R)-(-) Carvone	Sigma Aldrich	Cat#12,493-1
(S)-(+) Carvone	Sigma Aldrich	Cat#435759
2-coumaranone	Sigma Aldrich	Cat#12,459-1
2-isobutyl-3-Methoxypyrazine (IBMP)	Sigma Aldrich	Cat#297666
3,7-Dimethyl-2,6-Octadienenitrile (Citralva)	Sigma Aldrich	Cat#15,767-8
Acetophenone	Fluka	Cat#00790
Amersham Hybond P.045 PVDF	GE healthcare	Cat#10600023
BCA protein concentration assay kit	Thermo Scientific	Cat #23225
Benzaldehyde	Sigma Aldrich	Cat#41,809-9
Benzyl alcohol	Fluka	Cat#13170
Carbamoylcholine chrolide (Carbachol)	Sigma Aldrich	Cat#4382
Corning Nu Serum IV Culture Supplement	Life technologies	Cat# CB51000
Cytosine β-D-arabinofuranoside (Ara C)	Sigma Aldrich	Cat# C1768
DMEM high glucose	Life technologies	Cat#21969035
D-Valine	Sigma Aldrich	Cat#1255
Eugenol	Sigma Aldrich	Cat#E51791
Fetal Bovine Serum (FBS)	Life technologies	Cat#10270-106
Forskolin	Sigma Aldrich	Cat#F6886
Fura-2,AM	Life technologies	Cat#F1201
Geraniol	Fluka	Cat#48799
HEPES	Sigma Aldrich	Cat# H4034
Hank's balanced Salt solution (HBSS)	Life technologies	Cat#4180-046
High capacity cDNA Reverse Transcription kits	Applied Biosystems	Cat# 4368813
Heptanoic acid	Sigma Aldrich	Cat# 111-14-8
Hexanal	Sigma Aldrich	Cat#11,560-6
L- glutathione reduced	Sigma Aldrich	Cat#G4251
Lipofectamine 2000	Thermo Fisher	Cat#11668027
MEM alpha medium	Life technologies	Cat#32561-029
Menthone	Fluka	Cat#63680
Methyl salicylate	Sigma Aldrich	Cat#M6752
Nerve growth factor (NGF)	Corning	Cat#354009
Nonanedioci acid	Sigma Aldrich	Cat# 246379
NuPAGE4-12%Bis -Tris gel 1.0mm x 12 gel	Life technologies	Cat#NP0322BOX

(*Continued on next page*)

Continued

REAGENT or RESOURCE	SOURCE	IDENTIFIER
10% Pluronic acid	Life technologies	Cat# 24040-032
Pen Strep Glutamine (10X)	Life technologies	Cat#10378-96
Poly-L-Lysine solution	Sigma Aldrich	Cat#P8920
Propionic acid	Fluka	Cat#81912
Proteinase K	Life technologies	Cat#EO0491
Proteasi inhibitor cocktail	Sigma Aldrich	Cat#P8465
RIPA	Thermo Fisher	Cat#89901
SuperSignal ®West Pico Chemiluminescent substrate	Thermo Scientific	Cat#34040
Sulfinpyrazone	Sigma Aldrich	Cat# S9509
Tetrodotoxin (TTX)	Latoxan	Cat#L8503
Thrombin	Sigma Aldrich	Cat#T6884
TransFectin Lipid Reagent	Biorad	Cat#170-3350
Trizol	Life technologies	Cat#15596026
Vanillic acid	Sigma Aldrich	Cat#94770
Experimental Models: cell lines		
Human: HEK293T cells	ATCC	ATCC® CRL-3216; RRID:CVCL_0063
Experimental Models: Organisms/Strains		
Mouse: wild type C57BL/6J	Jackson Laboratory	Stock num#000664
Mouse: wild type C57BL/6-Tyr $^{c\text{-}Brd}$	Charles River	Strain code 493
Mouse: RKIP1 $^{Gt(pGT01xrBetageo)\ 1Jkl}$ (PEBP1$^{-/-}$)	Evan Keller	Michigan University
Mouse: P2-IRES-GFP (P2-GFP)	J.A Gogos	Columbia University
Mouse: Olfr160 $^{tm1.1(COP4*/EYFP)Tboz}$ /J (M72-ChR2-YFP)	Charles River	Cat#021206
Rat:Sprague Dawley	Charles River	Strain code 001
Recombinant DNA		
pCI	H. Matsunami	Duke University
OREG (MOR174-9) (Olfr73)	H. Matsunami	Duke University
P2 (MOR263-5)(Olfr17)	H. Matsunami	Duke University
S6 (MOR42-3) (Olfr544)	H. Matsunami	Duke University
Olfr62 (MOR 258-5)	H. Matsunami	Duke University
M72 (MOR171-3)(Olfr160)	H. Matsunami	Duke University
$G_{\alpha 15}$	H. Matsunami	Duke University
RTP1S	H. Matsunami	Duke University
RTP2	H. Matsunami	Duke University
pGEX2T-rat-RKIPcDNA	MR Rosner	Chicago University
mKate	Thermo Fisher	N/A
Epac-based sensor for cAMP	Ponsioen et al., 2004	N/A
Software and Algorithms		
MassLynx 4.1	Waters Corporation	N/A
MassHunter Qualitative Analysis Software B.03.01	Agilent Technologies	N/A
Mascot Search Engine 2.2.4	Matrix Science	N/A
ImageJ	NIH Software	RRID:nif-000030467
Prism 7.0	GraphPad Software	RRID: SCR_002798
Cell R	Olympus BioSystems	N/A
NRecon software	Bruker	N/A
Imaris	Bitplane	N/A
MATLAB	Mathworks	N/A

(*Continued on next page*)

Continued

REAGENT or RESOURCE	SOURCE	IDENTIFIER
Other		
Slide-A-Lyzer Dialysis cassette	Thermo Scientific	Cat#66330
HiTrap™ Benzamidine FF (High Sub)	GE Healthcare	Cat#17-5143-01
Glutathione Agarose	Jena Bioscience	Cat#AC-210-10
Superdex 200-prep-grade 300/10 column	GE Healthcare	Cat#S6782
HiTrap Capto Q column	GE Healthcare	Cat#11-0013-02
ImageQuant LAS 4000mini	GE healthcare	N/A
AKTA Fast protein Liquid Chromatography System	GE Healthcare	N/A
Jupiter C4 Column	Phenomenex	N/A
Electrospray ionization mass spectrometry with Q-TOF analyzer	Waters Corporation	N/A
Q-TOF mass spectrometer	Agilent Technologies	N/A
PV80 pneumatic PicoPump	WPI	Cat#SYS-PV820
Single Channel Pulse Generator (A310 Accupulser)	WPI	Cat#SYS-A310
Thermostatic chamber	Warner Instruments	N/A
Tissues lyzer II	Quiagen	N/A

LEAD CONTACT AND MATERIALS AVAILABILITY

Further information and requests for resources and reagents should be directed to and will be fulfilled by the Lead Contact, Claudia Lodovichi (claudia.lodovichi@unipd.it). This study did not generate new unique reagents.

EXPERIMENTAL MODEL AND SUBJECT DETAILS

Animals

Animals were housed in filtered cages in a temperature-controlled room, with 12/12 hour dark/light cycle with *ad libitum* access to water and food.

All procedures conformed to the EU Directive 2010/63/EU for animal experiments and to the ARRIVE guidelines. Experimental protocols were approved by the Italian Ministry of Health. All analyses were performed blind to genotype and treatment.

Experiments were performed on embryonic rat E18-19, on postnatal rats (P0-P4) (Sprague Dawley, Charles River), and on mice at age P0-P4 or P40-P50, according to the type of experiment, specified in the main text, both in males and females. The following lines of genetically modified mice were employed: P2-IRES-GFP mice (P2-GFP mice), generously provided by J.A. Gogos (Columbia University, New York, NY) and previously described in detail (Gogos et al., 2000); M72-ChR2-YFP mice (M72-YFP mice, Charles River); and PEBP1$^{-/-}$ mice (also known as RKIP1 $^{Gt(pGT01xrBetageo)\ 1Jkl}$), generously provided by Evan Keller, University of Michigan, and described in Theroux et al., 2007. We used C57BL/6 wild-type (WT) mice (Charles River) and C57BL/6-Tyr$^{c\text{-}Brd}$ mice (Charles River) as controls for PEBP1$^{-/-}$ mice.

Primary culture of rat and mouse olfactory sensory neurons

Primary cultures of rat and mouse OSNs were performed as described in Maritan et al. (2009) and Pietrobon et al. (2011). Briefly, the olfactory epithelium was harvested from embryonic rats (E18 - E19) in ice-cold Hank's balanced salt solution (HBSS) (Invitrogen). Then, the tissue was enzymatically dissociated (Maritan et al., 2009; Pietrobon et al., 2011). Cell suspension was plated onto 24mm coverslips coated with poly-L lysine (Sigma Aldrich) and maintained for 24 hours in culture medium D-Val MEM, 10% fetal bovine serum (FBS), 5% Nu Serum, Penstrep L-glutamine, 100 U/ml (Invitrogen), 10 μM Cytosine β-D-arabinofuranoside (Ara C, Sigma Aldrich), and 25 ng/ml nerve growth factor (NGF, Corning) before calcium imaging experiments or transfection with Epac-1 based sensor for cAMP (Ponsioen et al., 2004).

HEK293T cell culture

HEK293T cells were maintained in MEM (Invitrogen) containing 10% FBS and 1% Penstrep (Invitrogen) in a 37°C incubator with 5% CO_2. The cells were seeded on a 24 mm coverslip (Falcon) coated with poly-L-lysine (Sigma Aldrich) 24 hours prior to transfection. Lipofectamine 2000 (Invitrogen) was used for the transfection of 0.8 μg plasmid driving Rho-tagged OR expression (i.e., OREG, P2, S6, Olfr62, M72) and 0.4 μg of RTP1S, 0.4 μg of RTP2 and 0.8 μg of $G_{\alpha 15}$. HEK293T cells not expressing any OR transfected with the empty vector pCI, along with RTPs and $G_{\alpha 15}$, were used as controls and indicated as HEK cells transfected with pCI

or HEK cells not expressing OR in text and figures. The Rho-tagged OR and all the accessory plasmid DNA are described in detail in Zhuang and Matsunami (2007). mKate fluorescent protein (0.3 μg) (Thermo Fisher) was used as a control for transfection efficiency.

METHOD DETAILS

Isolation of olfactory bulb products

Olfactory bulbs (OB) were collected from rat embryos (E18 – E19) and frozen in liquid nitrogen. Frozen rat olfactory bulbs were powdered by pestle and mortar and lysed in a buffer containing 20 mM HEPES pH 7.4, 140 mM NaCl, 5 mM KCl, 5 mM $NaHCO_3$, 1.2 mM Na_2HPO_4, 1 mM $MgCl_2$, 20 mM HEPES pH 7.4, 10 mM dextrose, 1.8 mM $CaCl_2$, Roche Complete Protease Inhibitor Cocktail, 1 mM PMSF, 1 mM $NaVO_3$, 5 mM NaF and 3 mM β-glycerophosphate. The lysate was centrifuged to remove cell debris and membranes at 4°C for 30 minutes at 13000 rpm. Then, the supernatant was purified with a slide-A-lyzer dialysis cassette (cut off 350MW, Thermo Scientific) in 20mM HEPES and 100mM NaCl.

The dialyzed olfactory bulb extract was applied onto a HiTrap Desalting column (GE Healthcare), equilibrated with the elution buffer (20mM Tris pH 7.4 and 100mM NaCl). The proteins were eluted in a single peak and concentrated. They were purified by a Superdex 200 prep-grade 300/10 column (GE Healthcare), equilibrated with the elution buffer, and the resulting three peaks were separately collected (Size Exclusion Chromatography, SEC). The third peak (SEC-3), which elicited Ca^{2+} rises at the axon terminal in OSN, was adjusted to the composition of buffer A (20mM Tris, pH 8) and was loaded onto a HiTrap Capto Q column (GE Healthcare), equilibrated with buffer A (ionic exchange chromatography, IEC). The proteins that did not bind to the column were collected in fraction 1 (IEC-1). After washing the column with 10ml buffer A, a linear gradient (0%–30%) of buffer B (20mM Tris, 1M NaCl, pH 8) was applied and three peaks were collected (IEC- 2, −3 and −4). These chromatographic runs were performed with an AKTA Fast Protein Liquid Chromatography (FPLC) system (GE Healthcare).

Further High-Performance Liquid Cromatography (HPLC) analyses of the active fraction IEC-2 were conducted using reversed phase chromatography (RPC) using a Jupiter C4 column (4.6 mm x 150 mm; Phenomenex, CA, USA). Elution was done with a gradient of acetonitrile/0.085% TFA versus water/0.1% TFA from 5% to 38% in 5 minutes, from 38% to 43% in 15 minutes. The effluent was monitored by recording the absorbance at 226 nm. The products obtained in every step were concentrated and tested functionally as described above, peaks 23 and 35 were active.

Proteins were quantified using the Bradford assay. IEC-2 was heated at 99°C for 30 minutes to denature proteins in the sample (heated-IEC-2).

Identification of the eluted material from HPLC

The identity of active peaks 23 and 35 was assessed by mass spectrometry. Mass determinations were carried out with an electrospray ionization (ESI) mass spectrometer with a Q-TOF analyzer (Micro) from Waters Corporation (Manchester, UK). The measurements were conducted at a capillary voltage of 2.5 kV and a cone voltage of 30-35 V. The molecular masses of protein samples were estimated using the Mass-Lynx software 4.1 (Waters).

To identify the protein species, a fingerprinting analysis by trypsin was performed. Proteolysis with trypsin was conducted using an E/S ratio of 1:25 (by weight), in ammonium bicarbonate, pH 8, after reduction of disulfide bridges and carbamidomethylation of cysteine residues, and the reaction was quenched by acidification with TFA in water (4%, v/v). The tryptic digest mixture was analyzed by LC-MS/MS on a 6520 Q-TOF mass spectrometer (Agilent Technologies, Santa Clara, CA, USA) coupled to a chip-based chromatographic interface. A Large Capacity Chip (C18, 150 μm × 75 μm) with an enrichment column (C18, 9 mm, 160 nL volume) was used to separate peptides at a flow rate of 0.3 μl/min. Water/formic acid 0.1% and acetonitrile/formic acid 0.1% were used as eluents A and B, respectively. The chromatographic separation was achieved with a gradient of B from 5% to 50% in 20 minutes. Raw data files were converted into Mascot Generic Format (MGF) with MassHunter Qualitative Analysis Software version B.03.01 (Agilent Technologies) and analyzed with Mascot Search Engine version 2.2.4 (Matrix Science). MS/MS spectra were searched against the SwissProt database (version 2011-05, 528048 sequences). Enzyme specificity was set to trypsin/P with 1 missed cleavage, using a mass tolerance window of 1.2 Da for peptides and 0.6 Da for fragment ion matches. Carbamidomethylation of cysteine was set as fixed modification and methionine oxidation as variable modification. Proteins were considered as positive hits if at least 2 peptides per protein were identified with high confidence ($p < 0.05$).

Ca^{2+} imaging in olfactory sensory neurons and HEK293T cells

Ca^{2+} imaging was performed on OSNs of embryonic (E18-E19) rat and of postnatal day (P) P0-P4 mice and on HEK293T cells. The day of the experiment (~10 −12 hours after plating), neurons or HEK293T cells were loaded with 5 μM Fura 2 – AM (Life Technologies), 500 μM sulfinpyrazone (Sigma Aldrich) and 0.01% pluronic acid (Life Technologies) in medium at 37°C for 30 minutes. Coverslips were mounted in a thermostatic chamber at 37°C (Warner Instruments) and maintained in Ringer's solution (140mM NaCl, 5mM KCl, 1mM CaCl2 *$2H_2O$, 1mM $MgCl_2$, 10mM HEPES, 10mM glucose, 1mM sodium pyruvate, pH 7.2). OSNs and HEK293T cells were continuously perfused with the Ringer's Solution (3 ml/min) except during stimulus presentation. Experiments on OSNs were performed in the presence of 4 μM TTX (Latoxan) in order to avoid action potential contribution to the measured Ca^{2+} signal. The Ca^{2+} imaging experiments were performed on an inverted microscope IX 81 (Olympus) equipped with a UPlanFL 60X NA

1.25 oil immersion objective (Olympus), a xenon light source (150 W) for epifluorescence illumination, a 12-bit CCD camera (SIS F-View) and an illumination system MT20 (Olympus). Images were acquired every second (s) (for OSN) and every 3 s (for HEK293T cells) using 380/15 nm and 340/15 nm excitation filters and collected through a 510/40 nm emission filter (Olympus). Data were acquired with a Cell^R software and analyzed offline with the ImageJ software (NIH). Changes in fluorescence (340nm/380nm) were expressed as R/R_0 where R is the ratio at time t and R_0 is the ratio at time = 0 s. Amplitude of response was computed as $\Delta R/R_{min}$ (%), where $\Delta R = R_{max} - R_{min}$. Calcium responses with amplitude < 10% were excluded from the analysis. Ca^{2+} responses were computed at the axon terminal of each single OSN and on single HEK293T cells, identified by ROIs.

Percentage of responsive HEK293T cells was calculated as: number of HEK293T cells responsive to the corresponding-odor or carbachol and to molecules from the OB/ tot number of HEK293T cells responsive to the corresponding-odor or carbachol X 100. In case of HEK293T cells transfected with the P2 OR, carbachol (CCH) was employed as a vitality test, since P2 cognate-odor ligand is still unknown. For HEK293T cells transfected with empty vector pCI, i.e., not expressing any OR, only cells responsive to carbachol, used as cell vitality test, were considered for statistics. Percentage of responsive OSN was calculated as: number of OSN responsive to molecules from the OB/ tot number of OSN tested X 100.

Cyclic AMP imaging in olfactory sensory neurons

Cells were transiently transfected with the Epac – based sensor for cAMP (Ponsioen et al., 2004), using Transfectin transfection reagent (Biorad). After transfection, neurons were maintained in culture for an additional 10 - 12 h before FRET imaging experiments to allow the genetically encoded sensor to be expressed. Imaging experiments were performed on an inverted microscope Olympus IX 70 with PlanApo 60X NA 1.4 oil-immersion objective. Excitation at 430 nm was performed with a Polychrome IV monochromator (Till Photonics GmbH, Germany) equipped with a 150 W xenon lamp. Images were captured every 3 s with a 16-bit sCMOS pco.edge camera (pco imaging), and the emission wavelengths were separated with a dual - emission beam splitter (Multispec Microimager; Optical Insights) with a 505 nm dichroic filter and 480 ± 15 and 545 ± 20 nm emission filters for CFP and YFP, respectively. All filters and dichroics were from Chroma Technology. The system is controlled by a custom-made software. Exposure time was set to 200-300 ms. Data were processed offline with ImageJ software (National Institutes of Health).

FRET changes were measured as changes in the background - subtracted 480/545 nm fluorescence emission intensities on excitation at 430 nm and expressed as R/R_0, where R is the ratio at time t and R_0 is the ratio at time = 0 s.

Stimuli

Olfactory bulb products; size exclusion chromatography (SEC) peaks 1-3; ionic exchange chromatography (IEC) peaks 1-4, 0.6-0.8 μg /μl; and reverse phase chromatography (RPC) peaks, 0.1-0.3 μg /μl, were focally applied to the growth cone of OSNs in culture and on HEK293T cells by a single-puff pressure ejection (Pneumatic pico-pump, WPI) with a glass micropipette (3–5 μm tip diameter, puff duration = 1 s, amplitude = 5 psi). PEBP1 (0.8 μg /μl) was focally applied at the axon terminal of OSN by a glass pipette. For HEK293Tcells, PEBP1 was diluted to a final concentration of 0.02 μg /μl in the bath solution. PEBP1 was digested with proteinase K (Life Technologies) 10 mg/ml (PEBP1+Prot.K) for 1 hour and 30 minutes at 57°C with Tris-HCl 1M pH = 7.5. Cyclin-dependent kinase 2 (CDK2) was purified with the same procedure used to purify PEBP1. CDK2 was diluted to the final concentration of 0.02 μg /μl in the bath solution.

Odors were prepared as 1mM stock in Ringer's solution and diluted to a final concentration of 100 μM in the bath solution. Odors: vanillic acid (VA), nonanedioic acid (NA), 2-coumaranone (CMR), and methyl salicylate (MS). Other stimuli: Carbachol (CCH) 100 μM. Forskolin (FRSK) 25 μM. All chemicals were from Sigma. Stimuli, i.e., odors and molecules from the bulb, were presented in random order.

Time-lapse imaging of axon turning of rat olfactory sensory neurons

The day after plating, embryonic rat neurons (see methods for primary culture above) were stimulated with microscopic gradients of chemicals, produced as described in Lohof et al. (1992). Briefly, repetitive pulsatile ejection of picoliter volumes of solutions containing the chemical was applied through a micropipette (tip diameter = 1-2 μm). The pressure was applied with an electrically gated pressure application system (PV820 pneumatic PicoPump, WPI). Pulses of pressure level 4 psi, duration 20 ms were applied to the pipette at a frequency of 2 Hz using a pulse generator (A310 Accupulser, WPI). The micropipette was placed at a distance of about 100 μm from the center of the growth cone and at an angle of ~45° from the direction of axon extension.

The images were acquired every 10 s on an inverted microscope Olympus IX 70 equipped with a 16-bit sCMOS PCO.edge camera (PCO imaging) and a modified LWD NeoSPlan 50X/0.60 air objective (Olympus). The objective was modified applying a ring of LEDs in order to produce a source of light below the sample and to increase the resolution of the growth cone contours. To quantify the turning response, the angle between the position of the center of the growth cone at the onset and the position of the center of the growth cone at the end of the stimulation period (~1 h) period was computed in polar coordinates.

Stimulus concentrations in the glass pipette were: forskolin 5mM, odor mixture (citralva, citronellal, menthone, carvone, eugenol, geraniol, acetophenone, hexanal, benzyl alcohol, heptanoic acid, propionic acid, benzaldehyde, and IBMP (all from Sigma) 1mM in Ringer's solution, ionic exchange chromatography fraction 2 (IEC-2) 5 μg/μl, PEBP1 1 μg/μl. Ringer's solution was used as control.

Expression and purification of pGEX-RKIP-1 fusion protein

pGEX2T-rat-RKIP cDNA (Raf Kinase Inhibitor protein, RKIP also known as Phosphatidylethanolamine-binding protein 1, PEBP1) was kindly provided by MR Rosner, Department of Biol. Science, University of Chicago. The purification of RKIP-GST fusion protein was performed following the standard procedures according to Harper and Speicher (2011).

The purification of the glutathione S-transferase (GST)-tagged protein (pGEX-RKIP-1) was performed by Glutathione Affinity purification. *E. coli* BL21(DE3) cells were transformed with a pGEX-2T vector enclosing the RKIP-1 coding sequence. Cells were grown for 2–3 h at 37°C, then the temperature was decreased to 20°C prior to induction. Expression was induced with 1 mM IPTG at OD600 = 0.6 over-night at 20°C. Cells were harvested by centrifugation for 20 min at 4000 g at 4°C. Bacteria were suspended in 50 mm Tris-HCl pH 8.0, 500 mm NaCl, and 1 mm DTT (buffer A) supplemented with EDTA-free Complete Mini Protease Inhibitor Cocktail (Roche) and were lysed using a French pressure cell press. The lysate was centrifuged for 45 min at 12000 rpm (15500 g, on a Beckman Coulter TA-14-50 rotor) at 4°C, and the supernatant was filtered and applied to a GST-affinity column (GE Healthcare) equilibrated with buffer A. GST-RKIP1 was eluted using buffer A supplemented with 10 mm reduced glutathione. The fusion protein was cut over-night with thrombin (Sigma Aldrich), then the cleaved GST tag was removed by a second GST-affinity chromatography. Finally, thrombin was removed from the purified RKIP1 exploiting a HiTrap Benzamidine FF (GE Healthcare) column. The final protein was concentrated at ~2 mg/mL, aliquoted, flash frozen in liquid nitrogen, and stored at −80°C. In each step, samples were collected for 12% sodium dodecyl sulfate polyacrylamide gel electrophoresis (SDS-PAGE) to test the GST-tagged protein expression.

RT-PCR

Total RNA was extracted with Trizol reagent (Invitrogen) and isolated from embryonic and postnatal rat, WT mice and PEBP1 $^{-/-}$ OSN and from WT and PEBP1 $^{-/-}$ mice olfactory bulb (OB). Expression of PEBP1 was analyzed by reverse transcription polymerase chain reaction (RT-PCR). Total RNA was reverse-transcribed into single-stranded cDNA using the transcriptor high capacity cDNA Reverse Transcription kits (Applied Biosystems), following the manufacturer's instructions. β -actin was used as a control.

The following primers were used: PEBP1: 5′-TCATGAATAGACCAAGCAGCAT-3′; 5′ - CATGCTTTATACGACTTGACTG −3′. β-actin: 5′-CCCTGTGCTGCTCACC-3′ and 5′-GCACGATTTCC CTCTCAG-3′.

Western blot

Proteins from olfactory bulb of embryonic and postnatal rat, and wild-type (WT) and PEBP1 $^{-/-}$ mice were dissected and solubilized in RIPA lysis buffer (Invitrogen) + protease inhibitor cocktail (Sigma Aldrich). Heart and skin tissues were taken from WT and PEBP1 $^{-/-}$ mice as a positive and negative control, respectively. Tissues were fractioned by tissues lyzer II (Quiagen) for 2 cycles of 30 s each. Then, a centrifugation at 14000rpm at 4°C for 30minutes was performed. Protein concentration was determined using BCA protein concentration assay kit (Thermo Scientific), following the manufacturers' instructions. The primary antibodies used were rabbit anti-RKIP (1:800, Millipore) and mouse anti-β-Actin (1:5000, Life Technologies). The secondary antibodies used were horseradish peroxidase-conjugated anti-rabbit IgG (1:5000, GE Healthcare), horseradish peroxidase-conjugated anti-mouse IgG (1:5000, GE Healthcare) in PBS Tween-20 0.05% + 5% not fat dry milk (Sigma Aldrich) for 1.5 hours at RT. Then, the membranes (Amersham Hybond P.045 520 PVDF, GE healthcare) were incubated with a chemiluminescent substrate (Thermo Scientific), and the signals were digitally detected by ImageQuant LAS 4000mini (GE healthcare). The band intensities were quantified using ImageJ software (RRID: nif-000030467). Protein levels were normalized with β-actin (Sigma Aldrich).

Immunohistochemistry

Immunohistochemistry was performed on olfactory bulb (OB) sections (horizontal or coronal) of: C57BL/6 wild-type mice (WT, used as control), PEBP1 $^{-/-}$ mice, P2-GFP mice, M72-GFP mice, PEBP1 $^{-/-}$ X M72-GFP mice and PEBP1 $^{-/-}$ X P2-GFP mice, at postnatal day (P) > 40. Immunohistochemistry was also performed on coronal OB sections of rat embryos (E18) and of postnatal rats, postnatal day P0-P4, in control and PEBP1$^{-/-}$ mice. Animals were euthanized and then perfused with 0.9% saline followed by 4% paraformaldehyde in 1X PBS. Brains were dissected and olfactory bulb promptly removed, post-fixed overnight in 4% paraformaldehyde. Olfactory bulbs were sectioned at 40μm-60μm at the vibratome (Leica, VT 1000S) or at 25 μm at cryostat (Leica1860). Expression of PEBP1 was analyzed in C57BL/6 mice (Charles River) and C57BL/6-Tyr$^{c\text{-}Brd}$ (Charles River) as a control for PEBP1$^{-/-}$ mice. No differences in PEBP1 expression were observed between C57BL/6 wild-type and C57BL/6-Tyr$^{c\text{-}Brd}$, therefore the results were pooled together.

The primary antibodies used were goat anti-OMP (1:500, Wako Chemicals), rabbit anti-RKIP, also known as PEBP1 (1:200, Millipore). The primary antibodies were revealed with CY3-conjugated donkey anti-goat (1:500, Jackson ImmunoResearch), Alexa Fluor 488-conjugated donkey anti-goat (1:500, Jackson ImmunoResearch), and CY3-conjugated donkey anti-rabbit (1:500, Jackson ImmunoResearch). DAPI (1:50000, Invitrogen) was used as a nuclear counterstaining. Sections were mounted with Aqua-Poly/Mount (Polysciences), and images were acquired at the Zeiss LSM700 or Leica MZ16 microscopes. The signal intensity of PEBP1, background subtracted, were performed on the anterior, medial, lateral and posterior side of the olfactory bulb sections from embryonic and postnatal rats and WT and PEBP1$^{-/-}$ mice, using ImageJ software (RRID: nif-000030467).

Measurements of glomeruli position in the olfactory bulb

Whole mount olfactory bulb analysis

P2-GFP, P2-GFP; PEBP1 $^{+/-}$, P2-GFP; PEBP1 $^{-/-}$, M72-YFP, M72-YFP; PEBP1 $^{+/-}$, M72-YFP; PEBP1 $^{-/-}$ mice were transcardially perfused with 0.9% saline followed by 4%paraformaldehyde in 1 X PBS. Brains were promptly removed, and whole mount images of olfactory bulbs were taken at a stereo microscope (Leica MZ 16F). Lateral and medial views of the olfactory bulb, in P2-GFP,

P2-GFP; PEBP1 $^{+/-}$ and P2-GFP; PEBP1 $^{-/-}$ mice, and dorsal views of the olfactory bulb of M72-YFP, M72-YFP; PEBP1 $^{+/-}$ and M72-YFP; PEBP1 $^{-/-}$ mice, were taken to calculate medial, lateral and dorsal surface areas, computed off line using ImageJ software.

The same images were used to measure the position of the main glomeruli (glom) along the postero- anterior (P-A) and dorso-ventro-dorsal (V-D) axis, following cartesian coordinates y axis = a line parallel to the coronal plane that separates the olfactory bulb from the brain. The perpendicular to y axis correspond to the x axis. The dorso-ventral position of glomeruli was calculated along the y axis, while the antero-posterior position was computed along the X axis (see Figure S9). No differences were observed between the projections to the right and the left bulb. Therefore, glomeruli position data were pooled between right and left bulb.

3D reconstruction of cleared olfactory bulbs

Cubic cleared olfactory bulbs (Susaki et al., 2015) were imaged on an optical projection tomography (Sharpe et al., 2002) device like previously published (Kerstens et al., 2019). For the imaging a Nikon PlanApo 0.1 NA 2x lens was used together with a GFP filtersets. To separate specific signal in the glomeruli from the background, we used ilastik (employing a machine learning procedure) to segment each bulb. The background signal was used to visualize the bulb, and the specific GFP signal was used for the glomeruli. Consequently, we reconstructed the data using NRecon software (Bruker). We oriented the bulbs in Fiji/imagej (Schindelin et al., 2012) and employed Imaris (Bitplane) for visualization and measurements of the data. The glomeruli were segmented as spheres. For normalization and measurement of the glomeruli position, we manually added six landmarks (as spots) that define the most anterior point, the most posterior point, the most dorsal point, the most ventral point, the most medial point, and the most lateral point. These points were used to define the Anterior-posterior, the dorsal-ventral and the medial-lateral axes. The extracted coordinates of the glomeruli and the landmarks were analyzed in MATLAB (Mathworks) using a custom-made script to describe the relative position of the glomeruli in 3D. The results were put in graphs using Excel (Microsoft).

QUANTIFICATION AND STATISTICAL ANALYSIS

Statistical tests, sample size, and P values are listed in each figure legend

Data are presented as mean ± SEM. Normal distribution of the variables of interest was checked using the Shapiro-Wilk test. Statistical comparisons of pooled data were performed using two-tailed Student's t test. A *P value* of < 0.05 was considered statistically significant. For experiments in which more than 2 groups were compared, one-way ANOVA followed by post hoc Bonferroni correction was performed using Prism software.

DATA AND CODE AVAILABILITY

This study did not generate /analyze [datasets/code]